Journal of Computational Physics 467 (2022) 111448

Contents lists available at ScienceDirect

Journal of Computational Physics

www.elsevier.com/locate/jcp

Numerical approximations of flow coupled binary phase field crystal system: Fully discrete finite element scheme with second-order temporal accuracy and decoupling structure

Xiaofeng Yang [a,*], Xiaoming He [b]

[a] Department of Mathematics, University of South Carolina, Columbia, SC, 29208, USA
[b] Department of Mathematics, Missouri University of Science & Technology, Rolla, MO, 65409, USA

ARTICLE INFO

Article history:
Received 2 February 2022
Received in revised form 28 May 2022
Accepted 2 July 2022
Available online 14 July 2022

Keywords:
Binary crystal model
Phase-field
Three-phase
Fully-decoupled
Second-order accuracy
Unconditional energy stability

ABSTRACT

In this article, we first establish a new flow-coupled binary phase-field crystal model and prove its energy law. Then by using some newly introduced variables, we reformulate this three-phase model into an equivalent form, which makes it possible to construct a fully discrete linearized decoupling scheme with unconditional energy stability and second-order time accuracy to solve this model for the first time. The energy law of the reformulated model is also proved. Then we incorporate the explicit-IEQ (invariant energy quadratization) method for the nonlinear potentials, the projection method for the Navier-Stokes equations, the Crank-Nicolson method for time marching, and the finite element method for spatial discretization together to develop the fully discrete scheme for the reformulated and equivalent system. By using the nonlocal splitting technique, at each time step, only a few decoupled constant-coefficient elliptic equations are required to be solved, even though the original and reformulated models are much more complicated in the form. The developed algorithm is further proved to be unconditionally energy stable, and a detailed implementation process is also provided. Various numerical experiments in 2D and 3D are carried out to verify the effectiveness of the developed scheme, including the binary crystal growth under the action of shear flow and the sedimentation process of many binary particles.

1. Introduction

From the pioneering modeling work of Elder et al. in [10,8] to the present, an important application of the phase-field method, called the phase-field crystal model (PFC, for short), has attracted significant attention in simulating the growth of atomic crystals [49,25,26,35,51,50,46,37,38,18,4,2,9,12,23,1,11]. The framework of the PFC model is to introduce the so-called phase-field variable to represent the coarse-grained time average concentration field of atomic density and then postulate a phenomenological total free energy. Applying the energy variational method to the total free energy, the governing system of equations is then derived, either in the H^{-1} space (called Cahn-Hilliard dynamics, cf. [10,8]) or in the L^2 space (called the Allen-Cahn dynamics, cf. [49]).

* Corresponding author.
E-mail addresses: xfyang@math.sc.edu (X. Yang), hex@mst.edu (X. He).

https://doi.org/10.1016/j.jcp.2022.111448
0021-9991/

According to the number of phase-field variables used, the PFC models can be categorized into different types, such as a single-phase PFC model for pure material, i.e., one type of atom, and a binary-phase PFC model for binary alloys, i.e., two types of atoms. Since the single-phase PFC model only needs to use one phase-field variable, its free energy composition form is relatively simple, consisting of two parts, a linear part and a nonlinear part (double-well and/or vacancy potential). After using the variational approach, the derived governing system contains only one independent partial differential equation (PDE). In contrast, the binary PFC model needs to use two phase-field variables. Hence its total free energy not only includes the single-phase energy belonging to each phase-field variable, but also contains a special form of the coupling part. Consequently, the governing system of the binary PFC model contains two highly coupled and nonlinear PDEs, which is much more complicated than the classical single-phase PFC model. Hence, while the single-phase PFC model for pure material has been combined with the hydrodynamic equations (Navier-Stokes) to simulate different flow field dominant phenomena [25,26,35], it is not surprising to see that the coupling of the binary PFC model with the fluid dynamics and the corresponding numerical simulation are still open.

Therefore, in this article, we consider the modeling and the numerical approximation for the hydrodynamics coupled binary PFC system. Following the idea of the single-phase PFC model combined with hydrodynamic equations [25,35,26], we first establish the governing system by coupling the Navier-Stokes equation with the binary PFC model and then prove its energy law. Then we focus on constructing an effective numerical scheme for the newly proposed model. The algorithm design may face arduous challenges due to the highly complex coupling and nonlinearity of the model itself, especially when our goal is to develop a second-order time-accurate, linear, unconditional energy stable, and decoupled fully discrete algorithm. More precisely, the numerical challenges include: (i) how to decouple the two phase-field variables; (ii) how to decouple the flow field from the two phase-field variables to obtain an easy implementation; and (iii) how to develop an appropriate time-discrete method for the nonlinear cubic term to obtain the linear format. Here, difficulty (i) is the exclusive problem of the binary model, and difficulty (ii) is an exclusive problem of the fluid coupling model. And we aim to simultaneously address these three difficulties together with another two major goals: unconditional stability and second-order temporal accuracy.

There are several numerical schemes available for difficulty (iii), including the convex-splitting method [37,38,18,4,27], the implicit quadrature method [16], the stabilization method [31,45,14,19], the IEQ method [46,50,48], the scalar auxiliary method (SAV) method [49,51,50], etc. Finite element methods have also been developed to solve various phase field models [3,6,13,21,22,28]. However, even for the simpler flow-coupled single-phase PFC model, which has attracted much attention [25,35,26], the numerical difficulties (i) and (ii) have not been addressed simultaneously. And it is even more difficult to address them directly for the more complicated binary case. Thus, to the authors' best knowledge, so far none of the above traditional methods can achieve linearity, decoupling, second order accuracy in time, and unconditional stability for these sophisticated models at the same time. Hence, for the flow-coupled binary PFC model proposed in this paper, we aim to design the first fully discrete numerical scheme, which is capable of achieving all of these four desired properties simultaneously.

The key idea of the new scheme is the introduction of two auxiliary variables and special ordinary differential equations (ODEs). Using these tools, the original system is then reformulated into an equivalent form by using an ingenious coupling method. More precisely, one local auxiliary variable and its ODE are used to rewrite the nonlinear potential as a quadratic function. And the nonlocal auxiliary variable and its ODE are used to deal with the coupled nonlinear terms. The major advantage to achieve this equivalent system for the original model is that the unconditional energy stability can be easily obtained by using simple explicit methods to discretize nonlinear terms. The nonlocal auxiliary variable can also be used to decompose every discrete equation into several sub-equations with constant coefficients, so that each variable can be solved independently at each time step, thereby greatly improving the computational efficiency. These are the major motivations for us to pay the cost of formulation complexity to reformulate the original model, while the later numerical implementation of the reformulated model only needs to solve several decoupled constant-coefficient elliptic equations. It is worthwhile to trade off this cost for improving the efficiency of the numerical implementation of such a sophisticated model and achieving all the four desired properties discussed above.

For the above novel designs, we are inspired by the IEQ scheme developed for the no-flow version of the PFC model in [46,50]. And one distinguishing feature of the proposed scheme is the use of explicit discretization to deal with almost all nonlinear and coupled terms. Therefore, we call this technique an explicit-IEQ method. In the following, we will provide the significant differences between the new explicit-IEQ method and the IEQ method developed in [46,50]. First, the ideas to define the critical auxiliary variables are different. Second, the IEQ method developed in [46,50] is designed for the no-flow model, while the explicit-IEQ method developed in this article is for the flow coupled model. Third, the IEQ scheme in [46,50] needs to solve a linear system with variable coefficients at each time step, which generally results in higher computational costs. In contrast, the explicit-IEQ method developed in this article only requires solving a few completely decoupled, linear, and constant-coefficient equations. Hence it's more efficient. To the best of our knowledge, the scheme constructed in this article is the first fully discrete algorithm of the flow-coupled PFC model with all of these characteristics: linearity, decoupling, temporal second-order accuracy, unconditional energy stability, and constant coefficients.

The rest of the article is organized as follows. In Section 2, we formulate the flow-coupled binary PFC model and then reformulate it to an equivalent form, with the energy dissipation structure provided. In Section 3, the fully discrete finite element numerical scheme is constructed, and a detailed step-by-step implementation process is given. The solvability and unconditional energy stability will also be proven rigorously. In Section 4, using the developed scheme, various numerical

examples of 2D and 3D, including some benchmark examples, such as crystal growth process and sedimentation process of many particles, are further carried out to show its effectiveness. Finally, some concluding remarks are provided in Section 5.

2. Flow-coupled binary phase-field crystal model and its energy law

In this section, we will first propose and analyze a basic flow-coupled binary phase-field crystal model. Then, inspired by some observation in the analysis of the basic model, we will introduce several auxiliary variables to equivalently reformulate the model so that it is more convenient to construct the desired numerical scheme.

We first introduce some notations, which will be used in the rest of this article. We assume that the domain $\Omega \in \mathscr{R}^d, d = 2, 3$ is open, rectangular, smooth and bounded. For any two functions $\phi(\boldsymbol{x})$ and $\psi(\boldsymbol{x})$, their L^2-inner product on Ω is denoted by $(\phi, \psi) = \int_\Omega \phi(\boldsymbol{x})\psi(\boldsymbol{x})d\boldsymbol{x}$, and the L^2-norm of $\phi(\boldsymbol{x})$ is denoted by $\|\phi\| = (\phi, \phi)^{\frac{1}{2}}$.

2.1. The flow-coupled binary PFC model

We now develop a binary PFC model with fluid dynamic coupling for binary alloys. We define two phase-field variables $\phi_1, \phi_2 : \Omega \to R$ to describe the local atomic density field for each atom type. From the modeling work of the so-called Swift-Hohenburg energy postulated in [34,24,10,8,25,35,26,2,9,12,23,1,11], the total free energy of the binary PFC system (no flow case) reads as follows:

$$E(\phi_1, \phi_2) = \int_\Omega \big(L(\phi_1, \phi_2) + N(\phi_1, \phi_2)\big)d\boldsymbol{x}. \tag{2.1}$$

Here $L(\phi_1, \phi_2)$ is the linear part, which will lead to the linear terms in the PDE model, and $N(\phi_1, \phi_2)$ is the nonlinear part, which will lead to the non-linear terms in the PDE model:

$$L(\phi_1, \phi_2) = \frac{\phi_1}{2}L_1^2\phi_1 + \frac{\phi_2}{2}L_2^2\phi_2 + \frac{\phi_1}{2}L_{12}^2\phi_2, \tag{2.2}$$

$$N(\phi_1, \phi_2) = F(\phi_1) + F(\phi_2) + F_{vac}(\phi_1) + F_{vac}(\phi_2) + F_{couple}(\phi_1, \phi_2), \tag{2.3}$$

where L_1, L_2, and L_{12} are defined as

$$L_1 = \Delta + a_1,\ L_2 = \Delta + a_2,\ L_{12} = \Delta + a_{12}, \tag{2.4}$$

Δ is the Laplace operator, a_1 and a_2 represent the equilibrium distance between atoms of the same species, and a_{12} sets the distance between different species of atoms, $F(\psi) = \frac{1}{4}\psi^4 - \frac{\varepsilon}{2}\psi^2$ is the fourth-order nonlinear smoothing potential, $F_{vac}(\psi) = \frac{\beta}{3}(|\psi|^3 - \psi^3)$ is the cubic penalized vacancy potential (cf. [5,32,33]), $F_{couple}(\phi_1, \phi_2) = \frac{1}{2}\gamma\phi_1^2\phi_2^2$ is the coupling potential, and $\varepsilon, \beta, \gamma$ are all positive constants (see [8,11,2] for further discussion of how these parameters relate to material properties).

In the following Lemma, we show that the total free energy $E(\phi_1, \phi_2)$ is bounded from below, which is a very important feature. Otherwise, the energy decay characteristic is meaningless.

Lemma 2.1. *The free energy $E(\phi_1, \phi_2)$ is bounded from below.*

Proof. We first consider the linear part $\int_\Omega L(\phi_1, \phi_2)d\boldsymbol{x}$ and reformulate it to

$$\int_\Omega L(\phi_1, \phi_2)d\boldsymbol{x} = \frac{1}{2}\|L_1\phi_1\|^2 + \frac{1}{2}\|L_2\phi_2\|^2 + \frac{1}{2}(L_{12}\phi_1, L_{12}\phi_2). \tag{2.5}$$

By using the Cauchy–Schwarz inequality, we estimate the lower bound of the last term as

$$\begin{aligned}
(L_{12}\phi_1, L_{12}\phi_2) &= (L_{12}\phi_1 - L_1\phi_1, L_{12}\phi_2) + (L_1\phi_1, L_{12}\phi_2) \\
&= (L_{12}\phi_1 - L_1\phi_1, L_{12}\phi_2 - L_2\phi_2) + (L_{12}\phi_1 - L_1\phi_1, L_2\phi_2) \\
&\quad + (L_1\phi_1, L_{12}\phi_2 - L_2\phi_2) + (L_1\phi_1, L_2\phi_2) \\
&= (a_{12} - a_1)(a_{12} - a_2)(\phi_1, \phi_2) + (a_{12} - a_1)(\phi_1, L_2\phi_2) \\
&\quad + (a_{12} - a_2)(L_1\phi_1, \phi_2) + (L_1\phi_1, L_2\phi_2) \\
&\geq -\frac{|(a_{12} - a_1)(a_{12} - a_2)|}{2}\big(\|\phi_1\|^2 + \|\phi_2\|^2\big) - \frac{\zeta}{4}\|L_2\phi_2\|^2 - \frac{1}{\zeta}|a_{12} - a_1|^2\|\phi_1\|^2 \\
&\quad - \frac{\zeta}{4}\|L_1\phi_1\|^2 - \frac{1}{\zeta}|a_{12} - a_2|^2\|\phi_2\|^2 - \frac{1}{2}\|L_1\phi_1\|^2 - \frac{1}{2}\|L_2\phi_2\|^2.
\end{aligned} \tag{2.6}$$

Hence, combining with the nonlinear part, we deduce

$$\begin{aligned} E(\phi_1,\phi_2) &= \int_\Omega (L(\phi_1,\phi_2)+N(\phi_1,\phi_2))d\boldsymbol{x} \\ &\geq (\frac{1}{2}-\frac{\zeta}{4})\|L_1\phi_1\|^2+(\frac{1}{2}-\frac{\zeta}{4})\|L_2\phi_2\|^2 \\ &\quad+\int_\Omega \Big\{ F(\phi_1)+F(\phi_2)+\frac{1}{2}\gamma\phi_1^2\phi_2^2+\frac{\beta}{3}|\phi_1|^3+\frac{\beta}{3}|\phi_2|^3-\frac{\beta}{3}\phi_1^3-\frac{\beta}{3}\phi_2^3 \\ &\quad-\Big(\frac{|(a_{12}-a_1)(a_{12}-a_2)|}{2}+\frac{1}{\zeta}|a_{12}-a_1|^2\Big)|\phi_1|^2 \\ &\quad-\Big(\frac{|(a_{12}-a_1)(a_{12}-a_2)|}{2}+\frac{1}{\zeta}|a_{12}-a_2|^2\Big)|\phi_2|^2\Big\}d\boldsymbol{x}. \end{aligned} \tag{2.7}$$

It is easy to see that the terms in { } are bounded from below, since the fourth-order terms contained in $F(\phi_1)$ and $F(\phi_2)$ dominate all other negative terms from below. Therefore, as long as the constant ζ is set to satisfy $0<\zeta\leq 2$ (for example, we take $\zeta=1$), we deduce that $E(\phi_1,\phi_2)$ is bounded from below. □

Following the similar variational approach for deriving the flow-coupled single-phase PFC model given in [25,35,26], we propose the flow coupled binary-phase PFC model for binary alloys as follows:

$$\phi_{1t}+\nabla\cdot(\mathbf{u}\phi_1)=M\Delta\mu_1, \tag{2.8}$$

$$\mu_1=\lambda(L_1^2\phi_1+\frac{1}{2}L_{12}^2\phi_2+f(\phi_1)+f_{vac}(\phi_1)+\gamma\phi_1\phi_2^2), \tag{2.9}$$

$$\phi_{2t}+\nabla\cdot(\mathbf{u}\phi_2)=M\Delta\mu_2, \tag{2.10}$$

$$\mu_2=\lambda(L_2^2\phi_2+\frac{1}{2}L_{12}^2\phi_1+f(\phi_2)+f_{vac}(\phi_2)+\gamma\phi_1^2\phi_2), \tag{2.11}$$

$$\mathbf{u}_t+(\mathbf{u}\cdot\nabla)\mathbf{u}+\nabla p-\nu\Delta\mathbf{u}+\phi_1\nabla\mu_1+\phi_2\nabla\mu_2=0, \tag{2.12}$$

$$\nabla\cdot\mathbf{u}=0, \tag{2.13}$$

where $\mathbf{u}$ is the fluid velocity, p is the pressure, ν is the viscosity, $\mu_1=\frac{\delta E}{\delta\phi_1}$ and $\mu_2=\frac{\delta E}{\delta\phi_2}$ are the chemical potentials, $f(\psi)=F'(\psi)=\psi^3-\varepsilon\psi$, $f_{vac}(\psi)=F'_{vac}(\psi)=\beta(|\psi|-\psi)\psi$, M is the relaxation mobility, λ is a positive constant (see [26]). The equations for $\phi_1,\mu_1,\phi_2,\mu_2$ are derived by taking the variational gradient flow approach to the free energy $E(\phi_1,\phi_2)$ in the H^{-1} space, i.e., the Cahn-Hilliard dynamics.

Remark 2.1. We can also expand the two linear operators L_1^2 and L_2^2 in (2.9) and (2.11) to the following open format:

$$\begin{cases} \mu_1=\lambda(\Delta^2\phi_1+2a_1\Delta\phi_1+a_1^2\phi_1+\frac{1}{2}L_{12}^2\phi_2+f(\phi_1)+f_{vac}(\phi_1)+\gamma\phi_1\phi_2^2), \\ \mu_2=\lambda(\Delta^2\phi_2+2a_2\Delta\phi_2+a_2^2\phi_2+\frac{1}{2}L_{12}^2\phi_1+f(\phi_2)+f_{vac}(\phi_2)+\gamma\phi_1^2\phi_2). \end{cases} \tag{2.14}$$

Since we expect to establish a decoupling scheme, in Section 3, we will use this open format for the two linear operators L_1^2 and L_2^2.

The initial conditions of the system (2.8)-(2.13) read as

$$\mathbf{u}|_{(t=0)}=\mathbf{u}^0,\ \phi_1|_{(t=0)}=\phi_1^0,\phi_2|_{(t=0)}=\phi_2^0,\ p|_{(t=0)}=p^0. \tag{2.15}$$

We also consider the following boundary conditions:

$$\mathbf{u}|_{\partial\Omega}=\mathbf{0},\ \partial_{\mathbf{n}}\phi_1|_{\partial\Omega}=\partial_{\mathbf{n}}\phi_2|_{\partial\Omega}=\partial_{\mathbf{n}}\Delta\phi_1|_{\partial\Omega}=\partial_{\mathbf{n}}\Delta\phi_2|_{\partial\Omega}=\partial_{\mathbf{n}}\mu_1|_{\partial\Omega}=\partial_{\mathbf{n}}\mu_2|_{\partial\Omega}=0, \tag{2.16}$$

where $\mathbf{n}$ is the unit outward normal on the boundary. Note that it is also very common to assume that all variables meet periodic boundary conditions in the existing work, see [34,24,10,8,25,35,26,2,9,12,23,1,11,37,38,18,4,46,50].

It is easy to derive that the total free energy of the system (2.8)-(2.13) follows an energy dissipation law, which is shown in the following Lemma.

Lemma 2.2. *The PDE system (2.8)-(2.13) holds a law of energy dissipation:*

$$\frac{d}{dt}E_{tot}(\mathbf{u},\phi_1,\phi_2)=-M(\|\nabla\mu_1\|^2+\|\nabla\mu_2\|^2)-\nu\|\nabla\mathbf{u}\|^2\leq 0, \tag{2.17}$$

where

$$E_{tot}(\mathbf{u},\phi_1,\phi_2)=\frac{1}{2}\|\mathbf{u}\|^2+\lambda E(\phi_1,\phi_2). \tag{2.18}$$

Proof. First, taking the L^2 inner product of (2.8) with μ_1, of (2.9) with $-\phi_{1t}$, of (2.10) with μ_2, of (2.11) with $-\phi_{2t}$, using integration by parts and combining the four obtained equations, we obtain

$$\lambda\frac{d}{dt}\int_\Omega (L(\phi_1,\phi_2)+N(\phi_1,\phi_2))\,d\boldsymbol{x}=-M\|\nabla\mu_1\|^2-M\|\nabla\mu_2\|^2-(\nabla\cdot(\mathbf{u}\phi_1),\mu_1)-(\nabla\cdot(\mathbf{u}\phi_2),\mu_2). \tag{2.19}$$

Second, by taking the inner product of (2.11) with $\mathbf{u}$ in L^2, and using the divergence-free condition (2.12) and integration by parts, we derive

$$\frac{d}{dt}\int_\Omega\frac{1}{2}|\mathbf{u}|^2d\boldsymbol{x}=-\nu\|\nabla\mathbf{u}\|^2-((\mathbf{u}\cdot\nabla)\mathbf{u},\mathbf{u})-(\phi_1\nabla\mu_1,\mathbf{u})-(\phi_2\nabla\mu_2,\mathbf{u}). \tag{2.20}$$

By combining (2.19) and (2.20) and using (2.21) of Remark 2.2, we deduce the law of energy dissipation (2.17), where $E_{tot}(\mathbf{u},\phi_1,\phi_2)$ is the total free energy for the model (2.8)-(2.13). From Lemma 2.1, the total energy $E_{tot}(\mathbf{u},\phi_1,\phi_2)$ can be guaranteed to be bounded from below. □

Remark 2.2. Remarkably, in the process deriving (2.17), we utilize the following three equations:

$$(\nabla\cdot(\mathbf{u}\phi_i),\mu_i)+(\phi_i\nabla\mu_i,\mathbf{u})=0,i=1,2,\quad((\mathbf{u}\cdot\nabla)\mathbf{u},\mathbf{u})=0, \tag{2.21}$$

which can be verified by applying integration by parts, the boundary conditions of (2.16) and the divergence-free condition (2.13). In the energy law derivation process of Lemma 2.2, the final elimination of these three terms means that they will not have any impact on the energy law of the governing system. This feature of "zero-contribution-energy" (see also in [44,47,40,43,41,42]) prompts us to construct a scheme with a decoupling structure, as shown in the next section.

2.2. Equivalent reformulation of the model

As discussed in the introduction, none of the traditional methods can achieve linearity, decoupling, second order accuracy in time, and unconditional stability at the same time for the sophisticated target model of this paper. Therefore, in this paper we need to develop a new method, which additionally defines local/non-local variables inspired from various ideas and uses them to reconstruct the above PDE system into a desired form. This extra effort is particularly paid to overcome the major difficulty in designing the first fully discrete numerical scheme, which is capable of achieving all of the above four desired properties simultaneously for the flow-coupled binary PFC model proposed in this paper. On the other hand, the features of this reformulated model and our ideas of the new numerical scheme in the next section will eventually lead to solving a few decoupled constant-coefficient elliptic equations only at each time iteration step. That is, the extra effort and the complexity of the reformulated model is traded off for the efficiency of the numerical implementation and the algorithm's capability of simultaneously achieving the above four desired properties. Therefore, in this subsection we will first focus on the model reformulation by using the newly defined critical auxiliary variables.

First, in order to force the original energy potential to be "quadratic", which comes from the IEQ method developed for the no-flow version of the PFC model in [46,50], we define an auxiliary variable (local type) $U(\boldsymbol{x},t)$ as

$$U(\boldsymbol{x},t)=\sqrt{\frac{a_1^2}{2}\phi_1^2+\frac{a_2^2}{2}\phi_2^2+N(\phi_1,\phi_2)-\frac{S}{2}\phi_1^2-\frac{S}{2}\phi_2^2+B}, \tag{2.22}$$

where $S>0$ and $B>0$ are two predetermined constants. Note that the term in the square root, $\frac{a_1^2}{2}\phi_1^2+\frac{a_2^2}{2}\phi_2^2+N(\phi_1,\phi_2)-\frac{S}{2}\phi_1^2-\frac{S}{2}\phi_2^2$, is always bounded from below. This is because all the negative terms, including the cubic polynomial terms in $F_{vac}(\phi_1)$ and $F_{vac}(\phi_2)$, the negative quadratic terms related to S, and the negative quadratic terms in $F(\phi_1)$ and $F(\phi_2)$, can be always bounded by the fourth-order terms contained in $F(\phi_1)$ and $F(\phi_2)$ from below. The reason for using a predetermined constant B is that we are trying to make the term in the square root always positive.

Using the new variable $U(\boldsymbol{x},t)$ and defining $\psi_1=\Delta\phi_1,\psi_2=\Delta\phi_2,\Psi_1=L_{12}\phi_1,\Psi_2=L_{12}\phi_2$, we reformulate (2.8)-(2.11) as the following form:

$$\phi_{1t}+\nabla\cdot(\mathbf{u}\phi_1)=M\Delta\mu_1, \tag{2.23}$$

$$\mu_1=\lambda(\Delta\psi_1+2a_1\psi_1+\frac{1}{2}L_{12}\Psi_2+S\phi_1+H_1U), \tag{2.24}$$

$$\phi_{2t}+\nabla\cdot(\mathbf{u}\phi_2)=M\Delta\mu_2, \tag{2.25}$$

$$\mu_2 = \lambda(\Delta\psi_2 + 2a_2\psi_2 + \frac{1}{2}L_{12}\Psi_1 + S\phi_2 + H_2U), \tag{2.26}$$

$$\psi_1 = \Delta\phi_1, \psi_2 = \Delta\phi_2, \Psi_1 = L_{12}\phi_1, \Psi_2 = L_{12}\phi_2, \tag{2.27}$$

$$U_t = \frac{1}{2}(H_1\phi_{1t} + H_2\phi_{2t}), \tag{2.28}$$

$$U|_{(t=0)} = U(\boldsymbol{x}, 0), \tag{2.29}$$

where

$$\begin{cases} H_1 = \dfrac{a_1^2\phi_1 + f(\phi_1) + f_{vac}(\phi_1) + \gamma\phi_1\phi_2^2 - S\phi_1}{\sqrt{\frac{a_1^2}{2}\phi_1^2 + \frac{a_2^2}{2}\phi_2^2 + N(\phi_1,\phi_2) - \frac{S}{2}\phi_1^2 - \frac{S}{2}\phi_2^2 + B}}, \\ H_2 = \dfrac{a_2^2\phi_2 + f(\phi_2) + f_{vac}(\phi_2) + \gamma\phi_1^2\phi_2 - S\phi_2}{\sqrt{\frac{a_1^2}{2}\phi_1^2 + \frac{a_2^2}{2}\phi_2^2 + N(\phi_1,\phi_2) - \frac{S}{2}\phi_1^2 - \frac{S}{2}\phi_2^2 + B}}. \end{cases} \tag{2.30}$$

The equivalence between (2.8)-(2.11) and (2.23)-(2.29) is straightforward since a simple integration of (2.28) together with the initial condition (2.29) can recover (2.22). Therefore (2.9) and (2.11) are obtained by using (2.24) and (2.26).

Second, we introduce the most critical auxiliary variable $Q(t)$ (nonlocal type) for the effort of model reformulation, and define a special ODE for it:

$$\begin{cases} Q_t = ((\mathbf{u}\cdot\nabla)\mathbf{u}, \mathbf{u}) + (\nabla\cdot(\mathbf{u}\phi_1), \mu_1) + (\phi_1\nabla\mu_1, \mathbf{u}) + (\nabla\cdot(\mathbf{u}\phi_2), \mu_2) + (\phi_2\nabla\mu_2, \mathbf{u}) \\ \qquad + \lambda(H_1U, \phi_{1t}) - \lambda(H_1\phi_{1t}, U) + \lambda(H_2U, \phi_{2t}) - \lambda(H_2\phi_{2t}, U), \\ Q|_{(t=0)} = 1, \end{cases} \tag{2.31}$$

where the variables $\mathbf{u}, \phi_1, \mu_1, \phi_2, \mu_2$ follow the boundary conditions given in (2.16), and $\mathbf{u}$ also satisfies the divergence-free condition. Thus, from (2.21), it is easy to see that the ODE (2.31) is actually $Q_t = 0$, $Q|_{(t=0)} = 1$, which simply means a trivial solution of $Q(t) = 1$.

Remark 2.3. Note that all inner product terms contained in (2.31) cancel each other out in the continuous case. That is, the equation (2.31) is a trivial ODE ($Q_t = 0$) in the continuous case. However, this trivial ODE with such a special form can help us achieve the desired form of the algorithm that we expect in the discrete case, that is, a fully-decoupled scheme. By using different discrete methods for the two inner product terms that can cancel in the continuous case, we can simultaneously achieve second-order accuracy, full decoupling, linearity, and unconditional energy stability, as detailed below.

By replacing (2.9) and (2.11) with (2.24)-(2.29), and combining with the ODE (2.31) for Q, we get a new (but temporary) PDE system as

$$\phi_{1t} + \nabla\cdot(\mathbf{u}\phi_1) = M\Delta\mu_1, \tag{2.32}$$

$$\mu_1 = \lambda(\Delta\psi_1 + 2a_1\psi_1 + \frac{1}{2}L_{12}\Psi_2 + S\phi_1 + H_1U), \tag{2.33}$$

$$\phi_{2t} + \nabla\cdot(\mathbf{u}\phi_2) = M\Delta\mu_2, \tag{2.34}$$

$$\mu_2 = \lambda(\Delta\psi_2 + 2a_2\psi_2 + \frac{1}{2}L_{12}\Psi_1 + S\phi_2 + H_2U), \tag{2.35}$$

$$\psi_1 = \Delta\phi_1, \psi_2 = \Delta\phi_2, \Psi_1 = L_{12}\phi_1, \Psi_2 = L_{12}\phi_2, \tag{2.36}$$

$$U_t = \frac{1}{2}(H_1\phi_{1t} + H_2\phi_{2t}), \tag{2.37}$$

$$\begin{aligned} Q_t = {} & ((\mathbf{u}\cdot\nabla)\mathbf{u}, \mathbf{u}) + (\nabla\cdot(\mathbf{u}\phi_1), \mu_1) + (\phi_1\nabla\mu_1, \mathbf{u}) + (\nabla\cdot(\mathbf{u}\phi_2), \mu_2) + (\phi_2\nabla\mu_2, \mathbf{u}) \\ & + \lambda(H_1U, \phi_{1t}) - \lambda(H_1\phi_{1t}, U) + \lambda(H_2U, \phi_{2t}) - \lambda(H_2\phi_{2t}, U), \end{aligned} \tag{2.38}$$

$$\mathbf{u}_t + (\mathbf{u}\cdot\nabla)\mathbf{u} - \nu\Delta\mathbf{u} + \nabla p + \phi_1\nabla\mu_1 + \phi_2\nabla\mu_2 = 0, \tag{2.39}$$

$$\nabla\cdot\mathbf{u} = 0, \tag{2.40}$$

with $Q|_{(t=0)} = 1$ and $U|_{(t=0)} = U(\boldsymbol{x}, 0)$. It is straightforward to see that the new system (2.32)-(2.38) is equivalent to the original system (2.8)-(2.13).

Third, we reformulate the system (2.32)-(2.38) through the nonlocal variable Q into the following final form:

$$\phi_{1t} + \underbrace{Q\,\nabla\cdot(\mathbf{u}\phi_1)}_{\text{Q-reform}} = M\Delta\mu_1, \tag{2.41}$$

$$\mu_1 = \lambda(\Delta\psi_1 + 2a_1\psi_1 + \frac{1}{2}L_{12}\Psi_2 + S\phi_1 + \underbrace{Q\,H_1U}_{\text{Q-reform}}), \tag{2.42}$$

$$\phi_{2t} + \underbrace{Q\,\nabla\cdot(\mathbf{u}\phi_2)}_{\text{Q-reform}} = M\Delta\mu_2, \tag{2.43}$$

$$\mu_2 = \lambda(\Delta\psi_2 + 2a_2\psi_2 + \frac{1}{2}L_{12}\Psi_1 + S\phi_2 + \underbrace{Q\,H_2U}_{\text{Q-reform}}), \tag{2.44}$$

$$\psi_1 = \Delta\phi_1,\ \psi_2 = \Delta\phi_2,\ \Psi_1 = L_{12}\phi_1,\ \Psi_2 = L_{12}\phi_2, \tag{2.45}$$

$$U_t = \frac{1}{2}\underbrace{(Q\,H_1\phi_{1t} + Q\,H_2\phi_{2t})}_{\text{Q-reform}}, \tag{2.46}$$

$$\begin{aligned} Q_t = {} & ((\mathbf{u}\cdot\nabla)\mathbf{u},\mathbf{u}) + (\nabla\cdot(\mathbf{u}\phi_1),\mu_1) + (\phi_1\nabla\mu_1,\mathbf{u}) + (\nabla\cdot(\mathbf{u}\phi_2),\mu_2) + (\phi_2\nabla\mu_2,\mathbf{u}) \\ & +\lambda(H_1U,\phi_{1t}) - \lambda(H_1\phi_{1t},U) + \lambda(H_2U,\phi_{2t}) - \lambda(H_2\phi_{2t},U), \end{aligned} \tag{2.47}$$

$$\mathbf{u}_t + \underbrace{Q\,(\mathbf{u}\cdot\nabla)\mathbf{u}}_{\text{Q-reform}} - \nu\Delta\mathbf{u} + \nabla p + \underbrace{Q\,\phi_1\nabla\mu_1 + Q\,\phi_2\nabla\mu_2}_{\text{Q-reform}} = 0, \tag{2.48}$$

$$\nabla\cdot\mathbf{u} = 0, \tag{2.49}$$

with the boundary conditions

$$\mathbf{u}|_{\partial\Omega} = \mathbf{0},\ \partial_{\mathbf{n}}\phi_1|_{\partial\Omega} = \partial_{\mathbf{n}}\phi_2|_{\partial\Omega} = \partial_{\mathbf{n}}\Delta\phi_1|_{\partial\Omega} = \partial_{\mathbf{n}}\Delta\phi_2|_{\partial\Omega} = \partial_{\mathbf{n}}\mu_1|_{\partial\Omega} = \partial_{\mathbf{n}}\mu_2|_{\partial\Omega} = 0, \tag{2.50}$$

and the initial conditions

$$\mathbf{u}|_{(t=0)} = \mathbf{u}^0,\ \phi_1|_{(t=0)} = \phi_1^0,\ \phi_2|_{(t=0)} = \phi_2^0,\ p|_{(t=0)} = p^0,\ U|_{(t=0)} = U(\boldsymbol{x},0),\ Q\,|_{t=0} = 1. \tag{2.51}$$

Remark 2.4. In the process of the third reformatting to obtain (2.41)-(2.49), since $Q(t) = 1$, those under braced terms in (2.41)-(2.49) by multiplying with Q (marked as "Q-reform") will not be changed. Hence, from the detailed reformulation process mentioned above, it is easy to see that the finally obtained system (2.41)-(2.49) is equivalent to the original system (2.8)-(2.13).

In the following two lemmas, we show that the reformulated equivalent system (2.41)-(2.49) obeys the law of energy dissipation, and the total free energy is bounded from below.

Lemma 2.3. *The reformulated equivalent system* (2.41)-(2.49) *holds the law of energy dissipation as*

$$\frac{d}{dt}\hat{E}_{tot}(\phi_1,\phi_2,\psi_1,\psi_2,\Psi_1,\Psi_2,\mathbf{u},Q\,,U) = -M(\|\nabla\mu_1\|^2 + \|\nabla\mu_2\|^2) - \nu\|\nabla\mathbf{u}\|^2 \le 0, \tag{2.52}$$

where

$$\begin{aligned} \hat{E}_{tot}(\phi_1,\phi_2,\psi_1,\psi_2,\Psi_1,\Psi_2,\mathbf{u},Q\,,U) = {} & \frac{1}{2}\|\mathbf{u}\|^2 + \frac{1}{2}\lambda\Big\{\|\psi_1\|^2 + \|\psi_2\|^2 + (\Psi_1,\Psi_2) \\ & - 2a_1\|\nabla\phi_1\|^2 - 2a_2\|\nabla\phi_2\|^2 + S\|\phi_1\|^2 + S\|\phi_2\|^2\Big\} + \lambda\|U\|^2 + \frac{1}{2}|Q\,|^2 - \frac{1}{2} - B|\Omega|. \end{aligned} \tag{2.53}$$

Proof. By taking the inner product of (2.41) with μ_1 in L^2 and using integration by parts, we obtain

$$(\phi_{1t},\mu_1) = -M\|\nabla\mu_1\|^2 \underbrace{-Q\,(\nabla\cdot(\mathbf{u}\phi_1),\mu_1)}_{\text{I}_1}. \tag{2.54}$$

By taking the inner product of (2.42) with $-\phi_{1t}$ in L^2 and using integration by parts, we have

$$-(\mu_1,\phi_{1t}) = -\lambda(\psi_1,\Delta\phi_{1t}) - 2\lambda a_1(\psi_1,\phi_{1t}) - \frac{1}{2}\lambda(\Psi_2,L_{12}\phi_{1t}) - \frac{1}{2}\lambda\frac{d}{dt}(S\|\phi_1\|^2) \underbrace{-\lambda Q\,(H_1U,\phi_{1t})}_{\text{II}_1}. \tag{2.55}$$

By taking the L^2 inner product of (2.43) with μ_2 and using integration by parts, we derive

$$(\phi_{2t},\mu_2) = -M\|\nabla\mu_2\|^2 \underbrace{-Q\,(\nabla\cdot(\mathbf{u}\phi_2),\mu_2)}_{\text{III}_1}. \tag{2.56}$$

By taking the L^2 inner product of (2.44) with $-\phi_{2t}$ in L^2 and using integration by parts, we get

$$-(\mu_2,\phi_{2t}) = -\lambda(\psi_2,\Delta\phi_{2t}) - 2\lambda a_2(\psi_2,\phi_{2t}) - \frac{1}{2}\lambda(\Psi_1,L_{12}\phi_{2t}) - \frac{1}{2}\lambda\frac{d}{dt}(S\|\phi_2\|^2)\underbrace{-\lambda Q\,(H_2U,\phi_{2t})}_{\mathrm{IV}_1}. \tag{2.57}$$

By taking the time derivative of the four equations in (2.45), we have

$$\psi_{1t} = \Delta\phi_{1t}, \psi_{2t} = \Delta\phi_{2t}, \Psi_{1t} = L_{12}\phi_{1t}, \Psi_{2t} = L_{12}\phi_{2t}. \tag{2.58}$$

By taking the L^2 inner product for the first equation in (2.58) with $\lambda\psi_1$, and the second equation in (2.58) with $\lambda\psi_2$, we obtain

$$\frac{1}{2}\lambda\frac{d}{dt}\|\psi_1\|^2 = \lambda(\Delta\phi_{1t},\psi_1), \quad \frac{1}{2}\lambda\frac{d}{dt}\|\psi_2\|^2 = \lambda(\Delta\phi_{2t},\psi_2). \tag{2.59}$$

By taking the L^2 inner product of the third equation in (2.58) with $\frac{1}{2}\lambda\Psi_2$, of the fourth equation in (2.58) with $\frac{1}{2}\lambda\Psi_1$, we obtain

$$\frac{1}{2}\lambda(\Psi_{1t},\Psi_2) = \frac{1}{2}\lambda(L_{12}\phi_{1t},\Psi_2), \quad \frac{1}{2}\lambda(\Psi_{2t},\Psi_1) = \frac{1}{2}\lambda(L_{12}\phi_{2t},\Psi_1). \tag{2.60}$$

By taking the L^2 inner product of the first and second equation of (2.45) with $-2\lambda a_1\phi_{1t}$ and $-2\lambda a_2\phi_{2t}$, respectively, we get

$$-2\lambda a_1(\psi_1,\phi_{1t}) = \frac{1}{2}\lambda\frac{d}{dt}(2a_1\|\nabla\phi_1\|^2), \quad -2\lambda a_1(\psi_2,\phi_{2t}) = \frac{1}{2}\lambda\frac{d}{dt}(2a_2\|\nabla\phi_2\|^2). \tag{2.61}$$

By taking the inner product of (2.46) with $2\lambda U$, we obtain

$$\lambda\frac{d}{dt}\|U\|^2 = \lambda\underbrace{Q\,(H_1\phi_{1t},U)}_{\mathrm{V}_1} + \underbrace{\lambda Q\,(H_2\phi_{2t},U)}_{\mathrm{VI}_1}. \tag{2.62}$$

By taking the inner product of (2.48) with $\mathbf{u}$ in L^2, and using (2.49) and integration by parts, we obtain

$$\frac{d}{dt}\int_\Omega \frac{1}{2}|\mathbf{u}|^2 d\boldsymbol{x} = -\nu\|\nabla\mathbf{u}\|^2 \underbrace{-Q\,(\phi_1\nabla\mu_1,\mathbf{u})}_{\mathrm{VII}_1}\underbrace{-Q\,(\phi_2\nabla\mu_2,\mathbf{u})}_{\mathrm{VIII}_1}\underbrace{-Q\,((\mathbf{u}\cdot\nabla)\mathbf{u},\mathbf{u})}_{\mathrm{IX}_1}. \tag{2.63}$$

By multiplying (2.44) with Q, we obtain

$$\begin{aligned}\frac{d}{dt}\Big(\frac{1}{2}|Q|^2\Big) = &\underbrace{Q\,((\mathbf{u}\cdot\nabla)\mathbf{u},\mathbf{u})}_{\mathrm{IX}_2} + \underbrace{Q\,(\nabla\cdot(\mathbf{u}\phi_1),\mu_1)}_{\mathrm{I}_2} + \underbrace{Q\,(\phi_1\nabla\mu_1,\mathbf{u})}_{\mathrm{VII}_2} + \underbrace{Q\,(\nabla\cdot(\mathbf{u}\phi_2),\mu_2)}_{\mathrm{III}_2} + \underbrace{Q\,(\phi_2\nabla\mu_2,\mathbf{u})}_{\mathrm{VIII}_2}\\ &+\underbrace{\lambda Q\,(H_1U,\phi_{1t})}_{\mathrm{II}_2} - \underbrace{\lambda Q\,(H_1\phi_{1t},U)}_{\mathrm{V}_2} + \underbrace{\lambda Q\,(H_2U,\phi_{2t})}_{\mathrm{IV}_2} - \underbrace{\lambda Q\,(H_2\phi_{2t},U)}_{\mathrm{VI}_2}.\end{aligned} \tag{2.64}$$

After taking the combination of (2.54)-(2.57), (2.59)-(2.64), and noting that all terms under braced with the same Roman numerals (e.g., I_1 and I_2, etc.) are canceled out, we derive the energy dissipation law (2.52). □

Lemma 2.4. *If S satisfies the following condition*

$$S \geq max(\frac{3}{2}a_{12}^2 + 4a_1^2, \frac{3}{2}a_{12}^2 + 4a_2^2), \tag{2.65}$$

then the free energy $\hat{E}_{tot}(\phi_1,\phi_2,\psi_1,\psi_2,\Psi_1,\Psi_2,\mathbf{u},Q,U)$ given in (2.53) is bounded from below.

Proof. We only need to show that the terms in {} of (2.53) are bounded from below. First, similar to Lemma 2.1, we estimate the term (Ψ_1,Ψ_2) as follows by using the Cauchy-Schwarz inequality:

$$\begin{aligned}(\Psi_1,\Psi_2) &= (\Psi_1-\psi_1,\Psi_2) + (\psi_1,\Psi_2)\\ &= a_{12}^2(\phi_1,\phi_2) + a_{12}(\phi_1,\psi_2) + a_{12}(\psi_1,\phi_2) + (\psi_1,\psi_2)\\ &\geq -\frac{a_{12}^2}{2}\big(\|\phi_1\|^2+\|\phi_2\|^2\big) - \frac{\zeta}{4}\|\psi_2\|^2 - \frac{1}{\zeta}a_{12}^2\|\phi_1\|^2 - \frac{\zeta}{4}\|\psi_1\|^2 - \frac{1}{\zeta}a_{12}^2\|\phi_2\|^2 - \frac{1}{2}\|\psi_1\|^2 - \frac{1}{2}\|\psi_2\|^2.\end{aligned} \tag{2.66}$$

Second, we estimate the negative terms $-a_1\|\nabla\phi_1\|^2 - a_2\|\nabla\phi_2\|^2$ as follows

$$\begin{aligned}-2a_1\|\nabla\phi_1\|^2-2a_2\|\nabla\phi_2\|^2&=-2a_1(\nabla\phi_1,\nabla\phi_1)-2a_2(\nabla\phi_2,\nabla\phi_2)\\&=2a_1(\Delta\phi_1,\phi_1)+2a_2(\Delta\phi_2,\phi_2)\\&=2a_1(\psi_1,\phi_1)+2a_2(\psi_2,\phi_2)\\&\geq-\frac{\eta}{4}\|\psi_1\|^2-\frac{4}{\eta}a_1^2\|\phi_1\|^2-\frac{\eta}{4}\|\psi_2\|^2-\frac{4}{\eta}a_2^2\|\phi_2\|^2.\end{aligned}\tag{2.67}$$

Hence, we deduce

$$\begin{aligned}&\|\psi_1\|^2+\|\psi_2\|^2+(\Psi_1,\Psi_2)-2a_1\|\nabla\phi_1\|^2-2a_2\|\nabla\phi_2\|^2+S\|\phi_1\|^2+S\|\phi_2\|^2\\&\quad\geq(\frac{1}{2}-\frac{\zeta}{4}-\frac{\eta}{4})\|\psi_1\|^2+(\frac{1}{2}-\frac{\zeta}{4}-\frac{\eta}{4})\|\psi_2\|^2\\&\qquad+\big(S-\frac{a_{12}^2}{2}-\frac{1}{\zeta}a_{12}^2-\frac{4}{\eta}a_1^2\big)\|\phi_1\|^2+\big(S-\frac{a_{12}^2}{2}-\frac{1}{\zeta}a_{12}^2-\frac{4}{\eta}a_2^2\big)\|\phi_2\|^2.\end{aligned}\tag{2.68}$$

It is easy to see that the total free energy is bounded from below as long as the condition (2.65) is satisfied, which means we choose $\zeta=\eta=1$ in (2.68). □

Remark 2.5. The difference between the proof of the Lemma 2.2 and the proof of the Lemma 2.3 in the derivation of energy dissipation law fully explains why we need to transform the original system (2.8)-(2.13) to a new equivalent form (2.41)-(2.49) in such a special manner.

We take the advective term $\nabla\cdot(\mathbf{u}\phi_1)$ and the surface tension term $\phi_1\nabla\mu_1$ in the original system (2.8)-(2.13) as an example to illustrate the reason. In the process of Lemma 2.2, we notice that the inner product term $(\phi_1\nabla\mu_1,\mathbf{u})$ in (2.20) (term IV) will be offset by the term $(\nabla\cdot(\mathbf{u}\phi_1),\mu_1)$ (term I) contained in (2.19). This means that the discretization of the advective term $\nabla\cdot(\mathbf{u}\phi_1)$ and the surface tension $\phi_1\nabla\mu_1$ must be handled in some way, thereby leading to a coupled type scheme.

While for the newly modified system (2.41)-(2.49), in the Lemma 2.3, the term I_1 in (2.54) and VII_1 in (2.63) do not need to cancel each other, because the term I_2 in (2.64) can cancel I_1, and the term VII_2 in (2.64) can cancel VII_1. This means that when developing a numerical scheme, one can use different discretization methods to deal with the convection term $Q\nabla\cdot(\phi_1\mathbf{u})$ in (2.41) and the surface tension term $Q\phi_1\nabla\mu_1$ in (2.48), which makes it possible to build a complete decoupling type scheme.

3. Numerical methods

To construct a fully discrete numerical scheme for the flow coupled binary PFC system (2.8)-(2.12), we introduce a new method to realize the decoupled calculation. Instead of investigating each nonlinear term of the original model to distinguish whether to use implicit or explicit methods for discretization, the key idea is to discretize the above reformulated system.

3.1. Numerical scheme

In this subsection, we develop a fully-discrete algorithm for the system (2.41)-(2.49), which is an equivalent system of the hydrodynamically-coupled binary PFC model (2.8)-(2.13).

Some finite-dimensional discrete subspaces are introduced here. Suppose that the polygonal/polyhedral domain Ω is discretized by a conforming and shape regular triangulation/tetrahedron mesh $\mathcal{T}_h$ that is composed by open disjoint elements K such that $\bar{\Omega}=\bigcup_{K\in\mathcal{T}_h}\bar{K}$. We use $\mathcal{P}_l$ to denote the space of polynomials of total degree at most l and define the following finite element spaces:

$$\begin{aligned}&Y_h=\Big\{\phi\in C^0(\Omega):\phi|_K\in\mathcal{P}_{l_1}(K),\forall K\in\mathcal{T}_h\Big\},\ \boldsymbol{V}_h=\Big\{\boldsymbol{v}\in C^0(\Omega)^d:\boldsymbol{v}|_K\in\mathcal{P}_{l_2}(K)^d,\forall K\in\mathcal{T}_h\Big\}\cap H_0^1(\Omega)^d,\\&O_h=\Big\{q\in C^0(\Omega):q|_K\in\mathcal{P}_{l_2-1}(K),\forall K\in\mathcal{T}_h\Big\}\cap L_0^2(\Omega),\ X_h=\Big\{U\in C^0(\Omega):U|_K\in\mathcal{P}_{l_3}(K)^d,\forall K\in\mathcal{T}_h\Big\},\end{aligned}\tag{3.1}$$

where $H_0^1(\Omega)=\{u\in H^1(\Omega):u|_{\partial\Omega}=0\}$ and $L_0^2(\Omega)=\{q\in L^2(\Omega):\int_\Omega q dx=0\}$. Hence,

$$Y_h\subset H^1(\Omega),\boldsymbol{V}_h\subset H_0^1(\Omega)^d,O_h\subset L_0^2(\Omega),X_h\subset L^2(\Omega).\tag{3.2}$$

Besides, we assume the pair of spaces $(\boldsymbol{V}_h,O_h)$ satisfy the *inf-sup* condition [15]:

$$\beta\|q\|\leq\sup_{\boldsymbol{v}\in\boldsymbol{V}_h}\frac{(\nabla\cdot\boldsymbol{v},q)}{\|\nabla\boldsymbol{v}\|},\quad\forall q\in O_h,$$

where the constant β only depends on Ω.

The semi-discrete formulations of the system (2.41)-(2.49) in the weak form read as: find ϕ_1, μ_1, ϕ_2, μ_2, ψ_1, ψ_2, Ψ_1, $\Psi_2\in H^1(\Omega)$, $U\in L^2(\Omega)$, $\mathbf{u}\in H_0^1(\Omega)^d$, $p\in L_0^2(\Omega)$, such that

$$(\phi_{1t}, w_1) - Q(\mathbf{u}\phi_1, \nabla w_1) = -M(\nabla\mu_1, \nabla w_1), \tag{3.3}$$

$$(\mu_1, \Theta_1) = -\lambda(\nabla\psi_1, \nabla\Theta_1) + 2\lambda a_1(\psi_1, \Theta_1) + \frac{1}{2}\lambda(L_{12}^{\frac{1}{2}}\Psi_2, L_{12}^{\frac{1}{2}}\Theta_1) + \lambda S(\phi_1, \Theta_1) + \lambda Q(H_1U, \Theta_1), \tag{3.4}$$

$$(\phi_{2t}, w_2) - Q(\mathbf{u}\phi_2, \nabla w_2) = -M(\nabla\mu_2, \nabla w_2), \tag{3.5}$$

$$(\mu_2, \Theta_2) = -\lambda(\nabla\psi_2, \nabla\Theta_2) + 2\lambda a_2(\psi_2, \Theta_2) + \frac{1}{2}\lambda(L_{12}^{\frac{1}{2}}\Psi_1, L_{12}^{\frac{1}{2}}\Theta_2) + \lambda S(\phi_2, \Theta_2) + \lambda Q(H_2U, \Theta_2), \tag{3.6}$$

$$(\psi_1, \xi_1) = -(\nabla\phi_1, \nabla\xi_1), \qquad (\psi_2, \xi_2) = -(\nabla\phi_2, \nabla\xi_2), \tag{3.7}$$

$$(\Psi_1, \chi_1) = (L_{12}^{\frac{1}{2}}\phi_1, L_{12}^{\frac{1}{2}}\chi_1), \quad (\Psi_2, \chi_2) = (L_{12}^{\frac{1}{2}}\phi_2, L_{12}^{\frac{1}{2}}\chi_2), \tag{3.8}$$

$$(U_t, V) = \frac{1}{2}Q(H_1\phi_{1t}, V) + \frac{1}{2}Q(H_2\phi_{2t}, V), \tag{3.9}$$

$$\begin{aligned} Q_t = {} & ((\mathbf{u}\cdot\nabla)\mathbf{u}, \mathbf{u}) - (\mathbf{u}\phi_1, \nabla\mu_1) + (\phi_1\nabla\mu_1, \mathbf{u}) - (\mathbf{u}\phi_2, \nabla\mu_2) + (\phi_2\nabla\mu_2, \mathbf{u}) \\ & + \lambda(H_1U, \phi_{1t}) - \lambda(H_1\phi_{1t}, U) + \lambda(H_2U, \phi_{2t}) - \lambda(H_2\phi_{2t}, U), \end{aligned} \tag{3.10}$$

$$(\mathbf{u}_t, \boldsymbol{v}) + Q((\mathbf{u}\cdot\nabla)\mathbf{u}, \boldsymbol{v}) + \nu(\nabla\mathbf{u}, \nabla\boldsymbol{v}) - (p, \nabla\cdot\boldsymbol{v}) + Q(\phi_1\nabla\mu_1, \boldsymbol{v}) + Q(\phi_2\nabla\mu_2, \boldsymbol{v}) = 0, \tag{3.11}$$

$$(\nabla\cdot\mathbf{u}, q) = 0, \tag{3.12}$$

for $\Theta_1, w_1, \Theta_2, w_2, \xi_1, \xi_2, \chi_1, \chi_2 \in H^1(\Omega)$, $V \in L^2(\Omega)$, $\boldsymbol{v} \in H_0^1(\Omega)^d$, $q \in L_0^2(\Omega)$, where the linear operator associated with $L_{12}^{\frac{1}{2}}$ is defined as

$$(L_{12}^{\frac{1}{2}}\psi, L_{12}^{\frac{1}{2}}\Theta) = -(\nabla\psi, \nabla\Theta) + a_{12}(\psi, \Theta). \tag{3.13}$$

We let $\delta t > 0$ be a time step size and $t^n = n\delta t$ for $0 \le n \le N$ with $T = N\delta t$, and use ψ_h^n to denote the finite element approximation for the function $\psi(\cdot, t)$ at $t = t^n$. For convenience, we define $\tilde{\mathbf{u}}_h^{n+\frac{1}{2}} = \frac{1}{2}(\tilde{\mathbf{u}}_h^{n+1} + \mathbf{u}_h^n)$, and for any other variables Φ, we define $\bar{\Phi}^{n+\frac{1}{2}} = \frac{1}{2}(\Phi^{n+1} + \Phi^n)$.

Using the second-order Crank-Nicolson type formula for time marching, a fully discrete numerical scheme to solve the system (3.3)-(3.12) can be constructed as follows. Find ϕ_{1h}^{n+1}, μ_{1h}^{n+1}, ϕ_{2h}^{n+1}, μ_{2h}^{n+1}, ψ_{1h}^{n+1}, ψ_{2h}^{n+1}, Ψ_{1h}^{n+1}, $\Psi_{2h}^{n+1} \in Y_h$, $U_h^{n+1} \in X_h$, $\tilde{\mathbf{u}}_h^{n+1} \in \boldsymbol{V}_h$, $p_h^{n+1} \in O_h$, and one nonlocal scalar $Q^{n+1} \in \mathscr{R}$, such that

$$\left(\frac{\phi_{1h}^{n+1} - \phi_{1h}^n}{\delta t}, w_{1h}\right) - \bar{Q}^{n+\frac{1}{2}}(\mathbf{u}^*\phi_1^*, \nabla w_{1h}) = -M(\nabla\bar{\mu}_{1h}^{n+\frac{1}{2}}, \nabla w_{1h}), \tag{3.14}$$

$$\begin{aligned} (\bar{\mu}_{1h}^{n+\frac{1}{2}}, \Theta_{1h}) = {} & -\lambda(\nabla\bar{\psi}_{1h}^{n+\frac{1}{2}}, \nabla\Theta_{1h}) + 2\lambda a_1(\psi_1^*, \Theta_{1h}) \\ & + \frac{1}{2}\lambda(L_{12}^{\frac{1}{2}}\bar{\Psi}_{2h}^{n+\frac{1}{2}}, L_{12}^{\frac{1}{2}}\Theta_{1h}) + \lambda S(\bar{\phi}_{1h}^{n+\frac{1}{2}}, \Theta_{1h}) + \lambda\bar{Q}^{n+\frac{1}{2}}(H_1^*U^*, \Theta_{1h}), \end{aligned} \tag{3.15}$$

$$\left(\frac{\phi_{2h}^{n+1} - \phi_{2h}^n}{\delta t}, w_{2h}\right) - \bar{Q}^{n+\frac{1}{2}}(\mathbf{u}^*\phi_2^*, \nabla w_{2h}) = -M(\nabla\bar{\mu}_{2h}^{n+\frac{1}{2}}, \nabla w_{2h}), \tag{3.16}$$

$$\begin{aligned} (\bar{\mu}_{2h}^{n+\frac{1}{2}}, \Theta_{2h}) = {} & -\lambda(\nabla\bar{\psi}_{2h}^{n+\frac{1}{2}}, \nabla\Theta_{2h}) + 2\lambda a_2(\psi_2^*, \Theta_{2h}) \\ & + \frac{1}{2}\lambda(L_{12}^{\frac{1}{2}}\bar{\Psi}_{1h}^{n+\frac{1}{2}}, L_{12}^{\frac{1}{2}}\Theta_{2h}) + \lambda S(\bar{\phi}_{2h}^{n+\frac{1}{2}}, \Theta_{2h}) + \lambda\bar{Q}^{n+\frac{1}{2}}(H_2^*U^*, \Theta_{2h}), \end{aligned} \tag{3.17}$$

$$(\psi_{1h}^{n+1}, \xi_{1h}) = -(\nabla\phi_{1h}^{n+1}, \nabla\xi_{1h}), (\psi_{2h}^{n+1}, \xi_{2h}) = -(\nabla\phi_{2h}^{n+1}, \nabla\xi_{2h}), \tag{3.18}$$

$$(\Psi_{1h}^{n+1}, \chi_{1h}) = (L_{12}^{\frac{1}{2}}\phi_{1h}^{n+1}, L_{12}^{\frac{1}{2}}\chi_{1h}), \quad (\Psi_{2h}^{n+1}, \chi_{2h}) = (L_{12}^{\frac{1}{2}}\phi_{2h}^{n+1}, L_{12}^{\frac{1}{2}}\chi_{2h}), \tag{3.19}$$

$$\left(\frac{U_h^{n+1} - U_h^n}{\delta t}, V_h\right) = \frac{1}{2}\bar{Q}^{n+\frac{1}{2}}(H_1^*\phi_{1t}^*, V_h) + \frac{1}{2}\bar{Q}^{n+\frac{1}{2}}(H_2^*\phi_{2t}^*, V_h), \tag{3.20}$$

$$\begin{aligned} \frac{Q^{n+1} - Q^n}{\delta t} = {} & ((\mathbf{u}^*\cdot\nabla)\mathbf{u}^*, \tilde{\mathbf{u}}_h^{n+\frac{1}{2}}) - (\mathbf{u}^*\phi_1^*, \nabla\bar{\mu}_{1h}^{n+\frac{1}{2}}) + (\phi_1^*\nabla\mu_1^*, \tilde{\mathbf{u}}_h^{n+\frac{1}{2}}) \\ & - (\mathbf{u}^*\phi_2^*, \nabla\bar{\mu}_{2h}^{n+\frac{1}{2}}) + (\phi_2^*\nabla\mu_2^*, \tilde{\mathbf{u}}_h^{n+\frac{1}{2}}) + \lambda(H_1^*U^*, \frac{\phi_{1h}^{n+1} - \phi_{1h}^n}{\delta t}) - \lambda(H_1^*\phi_{1t}^*, \bar{U}^{n+\frac{1}{2}}) \\ & + \lambda(H_2^*U^*, \frac{\phi_{2h}^{n+1} - \phi_{2h}^n}{\delta t}) - \lambda(H_2^*\phi_{2t}^*, \bar{U}^{n+\frac{1}{2}}), \end{aligned} \tag{3.21}$$

$$\begin{aligned} & \left(\frac{\tilde{\mathbf{u}}_h^{n+1} - \mathbf{u}_h^n}{\delta t}, \boldsymbol{v}_h\right) + \bar{Q}^{n+\frac{1}{2}}((\mathbf{u}^*\cdot\nabla)\mathbf{u}^*, \boldsymbol{v}_h) + \nu(\nabla\tilde{\bar{\mathbf{u}}}_h^{n+\frac{1}{2}}, \nabla\boldsymbol{v}_h) + (\nabla p_h^n, \boldsymbol{v}_h) \\ & \quad + \bar{Q}^{n+\frac{1}{2}}(\phi_1^*\nabla\mu_1^*, \boldsymbol{v}_h) + \bar{Q}^{n+\frac{1}{2}}(\phi_2^*\nabla\mu_2^*, \boldsymbol{v}_h) = 0, \end{aligned} \tag{3.22}$$

$$(\nabla(p_h^{n+1}-p_h^n),\nabla q_h)=-\frac{2}{\delta t}(\nabla\cdot\tilde{\mathbf{u}}_h^{n+1},q_h), \tag{3.23}$$

$$\mathbf{u}_h^{n+1}=\tilde{\mathbf{u}}_h^{n+1}-\frac{\delta t}{2}(\nabla p_h^{n+1}-\nabla p_h^n), \tag{3.24}$$

for all $\Theta_{1h},w_{1h},\Theta_{2h},w_{2h},\xi_{1h},\xi_{2h},\chi_{1h},\chi_{2h}\in Y_h$, $V_h\in X_h$, $\boldsymbol{v}_h\in\boldsymbol{V}_h$, $q_h\in O_h$, where

$$\begin{cases}\mathbf{u}^*=\frac{3}{2}\mathbf{u}_h^n-\frac{1}{2}\mathbf{u}_h^{n-1},\phi_1^*=\frac{3}{2}\phi_{1h}^n-\frac{1}{2}\phi_{1h}^{n-1},\phi_2^*=\frac{3}{2}\phi_{2h}^n-\frac{1}{2}\phi_{2h}^{n-1},\\ \psi_1^*=\frac{3}{2}\psi_{1h}^n-\frac{1}{2}\psi_{1h}^{n-1},\psi_2^*=\frac{3}{2}\psi_{2h}^n-\frac{1}{2}\psi_{2h}^{n-1},\\ \mu_1^*=\frac{3}{2}\mu_{1h}^n-\frac{1}{2}\mu_{1h}^{n-1},\mu_2^*=\frac{3}{2}\mu_{2h}^n-\frac{1}{2}\mu_{2h}^{n-1},\\ H_1^*=H_1(\phi_1^*,\phi_2^*),H_2^*=H_2(\phi_1^*,\phi_2^*),\\ \phi_{1t}^*=\frac{\tilde{a}\phi_{1h}^n-\tilde{b}\phi_{1h}^{n-1}+\tilde{c}\phi_{1h}^{n-2}}{2\delta t},\phi_{2t}^*=\frac{\tilde{a}\phi_{2h}^n-\tilde{b}\phi_{2h}^{n-1}+\tilde{c}\phi_{2h}^{n-2}}{2\delta t},\tilde{a}=2,\tilde{b}=3,\tilde{c}=1.\end{cases} \tag{3.25}$$

Remark 3.1. In the above scheme (3.14)-(3.24), we adopt the time marching strategy based on the second-order Crank-Nicolson formula. All nonlinear terms are discretized using the second-order extrapolation method in turn, while the nonlocal auxiliary variable Q in (3.14), (3.15), (3.16), (3.17), (3.20), and (3.22) is discretized in an implicit manner, i.e., $\bar{Q}^{n+\frac{1}{2}}$. Meanwhile, the initialization of the scheme (3.14)-(3.24) requires the values of all variables at $t^1=\delta t,t^2=2\delta t$ which can be obtained by using the first-order scheme, namely, setting $\tilde{a}=\tilde{b}=2,\tilde{c}=0$ in practice.

Remark 3.2. The second-order pressure-correction scheme is used to decouple the computation of the pressure from that of the velocity. This projection method was analyzed in [29], where it is shown (discrete in time, continuous in space) that the scheme is second-order accurate for velocity but only first-order accurate for pressure. The loss of pressure accuracy is caused by the artificial Neumann boundary condition imposed on the pressure [7]. The final solution $\mathbf{u}_h^{n+1}$ satisfies the discrete divergence-free condition, which can be deduced by taking the L^2 inner product of (3.24) with $\nabla q_h\in O_h$, that is

$$(\mathbf{u}_h^{n+1},\nabla q_h)=(\tilde{\mathbf{u}}_h^{n+1},\nabla q_h)-\frac{\delta t}{2}(\nabla(p_h^{n+1}-p_h^n),\nabla q_h). \tag{3.26}$$

From the boundary condition of $\tilde{\mathbf{u}}_h^{n+1}$, we derive $(\tilde{\mathbf{u}}_h^{n+1},\nabla q_h)=-(\nabla\cdot\tilde{\mathbf{u}}_h^{n+1},q_h)$ by applying integration by parts. Therefore, from (3.23), we derive

$$(\mathbf{u}_h^{n+1},\nabla q_h)=0. \tag{3.27}$$

3.2. Decoupled implementation using the nonlocal splitting method

In this subsection, we introduce a nonlocal splitting method to obtain the decoupling implementation process for the scheme (3.14)-(3.24).

Step 1: using $\bar{Q}^{n+\frac{1}{2}}$, we split $\phi_{1h}^{n+1},\mu_{1h}^{n+1},\phi_{2h}^{n+1},\mu_{2h}^{n+1},\psi_{1h}^{n+1},\psi_{2h}^{n+1},\Psi_{1h}^{n+1},\Psi_{2h}^{n+1}$ into a linear combination form as

$$\begin{cases}\phi_{1h}^{n+1}=\phi_{11h}^{n+1}+\bar{Q}^{n+\frac{1}{2}}\phi_{12h}^{n+1},\quad \mu_{1h}^{n+1}=\mu_{11h}^{n+1}+\bar{Q}^{n+\frac{1}{2}}\mu_{12h}^{n+1},\\ \phi_{2h}^{n+1}=\phi_{21h}^{n+1}+\bar{Q}^{n+\frac{1}{2}}\phi_{22h}^{n+1},\quad \mu_{2h}^{n+1}=\mu_{21h}^{n+1}+\bar{Q}^{n+\frac{1}{2}}\mu_{22h}^{n+1},\\ \psi_{1h}^{n+1}=\psi_{11h}^{n+1}+\bar{Q}^{n+\frac{1}{2}}\psi_{12h}^{n+1},\quad \psi_{2h}^{n+1}=\psi_{21h}^{n+1}+\bar{Q}^{n+\frac{1}{2}}\psi_{22h}^{n+1},\\ \Psi_{1h}^{n+1}=\Psi_{11h}^{n+1}+\bar{Q}^{n+\frac{1}{2}}\Psi_{12h}^{n+1},\quad \Psi_{2h}^{n+1}=\Psi_{21h}^{n+1}+\bar{Q}^{n+\frac{1}{2}}\Psi_{22h}^{n+1}.\end{cases} \tag{3.28}$$

We solve ϕ_{ih}^{n+1}, μ_{ih}^{n+1}, ψ_{ih}^{n+1}, Ψ_{ih}^{n+1} for $i=1,2$, as follows.

Using (3.28), we replace $\phi_{ih}^{n+1},\mu_{ih}^{n+1},\psi_{ih}^{n+1},\Psi_{ih}^{n+1},i=1,2$ in the system (3.14)-(3.19), and decompose the obtained equations according to $\bar{Q}^{n+\frac{1}{2}}$ into the following four subsystems:

$$\begin{cases}\frac{1}{\delta t}(\phi_{11h}^{n+1},w_{1h})+\frac{1}{2}M(\nabla\mu_{11h}^{n+1},\nabla w_{1h})=G_1,\\ (\mu_{11h}^{n+1},\Theta_{1h})=-\lambda(\nabla\psi_{11h}^{n+1},\nabla\Theta_{1h})+\frac{1}{2}\lambda(L_{12}^{\frac{1}{2}}\Psi_{21h}^{n+1},L_{12}^{\frac{1}{2}}\Theta_{1h})+\lambda S(\phi_{11h}^{n+1},\Theta_{1h})+G_2,\\ (\psi_{11h}^{n+1},\xi_{1h})=-(\nabla\phi_{11h}^{n+1},\nabla\xi_{1h}),(\Psi_{21h}^{n+1},\chi_{2h})=(L_{12}^{\frac{1}{2}}\phi_{21h}^{n+1},L_{12}^{\frac{1}{2}}\chi_{2h}),\end{cases} \tag{3.29}$$

$$\begin{cases} \frac{1}{\delta t}(\phi_{12h}^{n+1}, w_{1h}) + \frac{1}{2}M(\nabla\mu_{12h}^{n+1}, \nabla w_{1h}) = (\mathbf{u}^*\phi_1^*, \nabla w_{1h}), \\ (\mu_{12h}^{n+1}, \Theta_{1h}) = -\lambda(\nabla\psi_{12h}^{n+1}, \nabla\Theta_{1h}) + \frac{1}{2}\lambda(L_{12}^{\frac{1}{2}}\Psi_{22h}^{n+1}, L_{12}^{\frac{1}{2}}\Theta_{1h}) + \lambda S(\phi_{12h}^{n+1}, \Theta_{1h}) + 2\lambda(H_1^*U^*, \Theta_{1h}), \\ (\psi_{12h}^{n+1}, \xi_{1h}) = -(\nabla\phi_{12h}^{n+1}, \nabla\xi_{1h}), (\Psi_{22h}^{n+1}, \chi_{2h}) = (L_{12}^{\frac{1}{2}}\phi_{22h}^{n+1}, L_{12}^{\frac{1}{2}}\chi_{2h}), \end{cases} \tag{3.30}$$

$$\begin{cases} \frac{1}{\delta t}(\phi_{21h}^{n+1}, w_{2h}) + \frac{1}{2}M(\nabla\mu_{21h}^{n+1}, \nabla w_{2h}) = G_3, \\ (\mu_{21h}^{n+1}, \Theta_{2h}) = -\lambda(\nabla\psi_{21h}^{n+1}, \nabla\Theta_{2h}) + \frac{1}{2}\lambda(L_{12}^{\frac{1}{2}}\Psi_{11h}^{n+1}, L_{12}^{\frac{1}{2}}\Theta_{2h}) + \lambda S(\phi_{11h}^{n+1}, \Theta_{1h}) + G_4, \\ (\psi_{21h}^{n+1}, \xi_{2h}) = -(\nabla\phi_{21h}^{n+1}, \nabla\xi_{2h}), (\Psi_{11h}^{n+1}, \chi_{1h}) = -(L_{12}^{\frac{1}{2}}\phi_{11h}^{n+1}, L_{12}^{\frac{1}{2}}\chi_{1h}), \end{cases} \tag{3.31}$$

$$\begin{cases} \frac{1}{\delta t}(\phi_{22h}^{n+1}, w_{2h}) + \frac{1}{2}M(\nabla\mu_{22h}^{n+1}, \nabla w_{2h}) = (\mathbf{u}^*\phi_2^*, \nabla w_{2h}), \\ (\mu_{22h}^{n+1}, \Theta_{2h}) = -\lambda(\nabla\psi_{22h}^{n+1}, \nabla\Theta_{2h}) + \frac{1}{2}\lambda(L_{12}^{\frac{1}{2}}\Psi_{12h}^{n+1}, L_{12}^{\frac{1}{2}}\Theta_{2h}) + \lambda S(\phi_{22h}^{n+1}, \Theta_{2h}) + 2\lambda(H_2^*U^*, \Theta_{2h}), \\ (\psi_{22h}^{n+1}, \xi_{2h}) = -(\nabla\phi_{22h}^{n+1}, \nabla\xi_{2h}), (\Psi_{12h}^{n+1}, \chi_{1h}) = (L_{12}^{\frac{1}{2}}\phi_{12h}^{n+1}, L_{12}^{\frac{1}{2}}\chi_{1h}), \end{cases} \tag{3.32}$$

where

$$\begin{cases} G_1 = \frac{1}{\delta t}(\phi_{1h}^n, w_{1h}) - \frac{1}{2}M(\nabla\mu_{1h}^n, \nabla w_{1h}), \\ G_2 = -(\mu_{1h}^n, \Theta_{1h}) - \lambda(\nabla\psi_{1h}^n, \nabla\Theta_{1h}) + \frac{1}{2}\lambda(L_{12}^{\frac{1}{2}}\Psi_{2h}^n, L_{12}^{\frac{1}{2}}\Theta_{1h}) + \lambda S(\phi_{1h}^n, \Theta_{1h}) + 4\lambda a_1(\psi_1^*, \Theta_{1h}), \\ G_3 = \frac{1}{\delta t}(\phi_{2h}^n, w_{2h}) - \frac{1}{2}M(\nabla\mu_{2h}^n, \nabla w_{2h}), \\ G_4 = -(\mu_{2h}^n, \Theta_{2h}) - \lambda(\nabla\psi_{2h}^n, \nabla\Theta_{2h}) + \frac{1}{2}\lambda(L_{12}^{\frac{1}{2}}\Psi_{1h}^n, L_{12}^{\frac{1}{2}}\Theta_{2h}) + \lambda S(\phi_{2h}^n, \Theta_{2h}) + 4\lambda a_2(\psi_2^*, \Theta_{2h}). \end{cases} \tag{3.33}$$

Note that (3.29) and (3.31) are coupled together, and so are (3.30) and (3.32). The following tips can help us realize their decoupling calculations. We take (3.29) and (3.31) as an example to describe the process.

We define

$$\begin{cases} \phi_a = \phi_{11h}^{n+1} + \phi_{21h}^{n+1}, \psi_a = \psi_{11h}^{n+1} + \psi_{21h}^{n+1}, \Psi_a = \Psi_{11h}^{n+1} + \Psi_{21h}^{n+1}, \mu_a = \mu_{11h}^{n+1} + \mu_{21h}^{n+1}, \\ \phi_b = \phi_{11h}^{n+1} - \phi_{21h}^{n+1}, \psi_b = \psi_{11h}^{n+1} - \psi_{21h}^{n+1}, \Psi_b = \Psi_{11h}^{n+1} - \Psi_{21h}^{n+1}, \mu_b = \mu_{11h}^{n+1} - \mu_{21h}^{n+1}. \end{cases} \tag{3.34}$$

We choose $w_{1h} = w_{2h} = w_h$, $\Theta_{1h} = \Theta_{2h} = \Theta_h$, $\xi_{1h} = \xi_{2h} = \xi_h$, $\chi_{1h} = \chi_{2h} = \chi_h$ and add (3.29) and (3.31) together to form the following two decoupled systems:

$$\begin{cases} \frac{1}{\delta t}(\phi_a, w_h) + \frac{1}{2}M(\nabla\mu_a, \nabla w_h) = G_1 + G_3, \\ (\mu_a, \Theta_h) = -\lambda(\nabla\psi_a, \nabla\Theta_h) + \frac{1}{2}\lambda(L_{12}^{\frac{1}{2}}\Psi_a, L_{12}^{\frac{1}{2}}\Theta_h) + \lambda S(\phi_a, \Theta_h) + G_2 + G_4, \\ (\psi_a, \xi_h) = -(\nabla\phi_a, \nabla\xi_h), (\Psi_a, \chi_h) = (L_{12}^{\frac{1}{2}}\phi_a, L_{12}^{\frac{1}{2}}\chi_h), \end{cases} \tag{3.35}$$

$$\begin{cases} \frac{1}{\delta t}(\phi_b, w_h) + \frac{1}{2}M(\nabla\mu_b, \nabla w_h) = G_1 - G_3, \\ (\mu_b, \Theta_h) = -\lambda(\nabla\psi_b, \nabla\Theta_h) - \frac{1}{2}\lambda(L_{12}^{\frac{1}{2}}\Psi_b, L_{12}^{\frac{1}{2}}\Theta_h) + \lambda S(\phi_b, \Theta_h) + G_2 - G_4, \\ (\psi_b, \xi_h) = -(\nabla\phi_b, \nabla\xi_h), (\Psi_b, \chi_h) = (L_{12}^{\frac{1}{2}}\phi_b, L_{12}^{\frac{1}{2}}\chi_h). \end{cases} \tag{3.36}$$

These two decoupled systems can be solved independently. Once we obtain the solution of them, we can update $\phi_{11h}^{n+1}, \phi_{21h}^{n+1}, \psi_{11h}^{n+1}, \psi_{21h}^{n+1}, \Psi_{11h}^{n+1}, \Psi_{21h}^{n+1}, \mu_{11h}^{n+1}, \mu_{21h}^{n+1}$ from (3.34) (for example, $\phi_{11h}^{n+1} = \frac{\phi_a+\phi_b}{2}$, $\phi_{21h}^{n+1} = \frac{\phi_a-\phi_b}{2}$). (3.30) and (3.32) can be solved in the similar manner. For the sake of brevity, we omit the details here.

Step 2: using $\bar{Q}^{n+\frac{1}{2}}$, we split U_h^{n+1} into a linear combination form as

$$U_h^{n+1} = U_{1h}^{n+1} + \bar{Q}^{n+\frac{1}{2}}U_{2h}^{n+1}. \tag{3.37}$$

We then decompose (3.20) into the following two equations:

$$(\frac{U_{1h}^{n+1}}{\delta t}, V_h) = (\frac{U_h^n}{\delta t}, V_h), \tag{3.38}$$

$$(\frac{U_{2h}^{n+1}}{\delta t}, V_h) = \frac{1}{2}(H_1^*\phi_{1t}^*, V_h) + \frac{1}{2}(H_2^*\phi_{2t}^*, V_h). \tag{3.39}$$

These two equations are easy to solve because all the terms on the right are known.

Step 3: using $\bar{Q}^{n+\frac{1}{2}}$, we split $\tilde{\mathbf{u}}_h^{n+1}$ into a linear combination form as

$$\tilde{\mathbf{u}}_h^{n+1} = \tilde{\mathbf{u}}_{1h}^{n+1} + \bar{Q}^{n+\frac{1}{2}} \tilde{\mathbf{u}}_{2h}^{n+1}. \tag{3.40}$$

We solve $\tilde{\mathbf{u}}_{1h}^{n+1}, \tilde{\mathbf{u}}_{2h}^{n+1}$ as follows.

$$(\frac{\tilde{\mathbf{u}}_{1h}^{n+1}}{\delta t}, \boldsymbol{v}_h) + \frac{1}{2}\nu(\nabla\tilde{\mathbf{u}}_{1h}^{n+1}, \nabla\boldsymbol{v}_h) = (\frac{\mathbf{u}_h^n}{\delta t}, \boldsymbol{v}_h) - \frac{1}{2}\nu(\nabla\mathbf{u}_h^n, \nabla\boldsymbol{v}_h) - (\nabla p_h^n, \boldsymbol{v}_h), \tag{3.41}$$

$$(\frac{\tilde{\mathbf{u}}_{2h}^{n+1}}{\delta t}, \boldsymbol{v}_h) + \frac{1}{2}\nu(\nabla\tilde{\mathbf{u}}_{2h}^{n+1}, \nabla\boldsymbol{v}_h) = -((\mathbf{u}^*\cdot\nabla)\mathbf{u}^*, \boldsymbol{v}_h) - (\phi_1^*\nabla\mu_1^*, \boldsymbol{v}_h) - (\phi_2^*\nabla\mu_2^*, \boldsymbol{v}_h). \tag{3.42}$$

It is very easy to solve (3.41) and (3.42), since they are linear and elliptic equations with only constant coefficients.

Step 4: we solve $\bar{Q}^{n+\frac{1}{2}}$ in (3.21). By using the linear combination forms for the variables ϕ_{1h}^{n+1}, μ_{1h}^{n+1}, ϕ_{2h}^{n+1}, μ_{2h}^{n+1}, U_h^{n+1}, $\tilde{\mathbf{u}}_h^{n+1}$ in (3.28), (3.37), (3.40), we formulate (3.21) into the following form:

$$(\frac{2}{\delta t} - \eta_2)\bar{Q}^{n+\frac{1}{2}} = \frac{2}{\delta t}Q^n + \eta_1, \tag{3.43}$$

where we use $Q^{n+1} - Q^n = 2(\bar{Q}^{n+\frac{1}{2}} - Q^n)$, and $\eta_i, i = 1, 2$ are given by

$$\begin{cases} \eta_1 = ((\mathbf{u}^*\cdot\nabla)\mathbf{u}^*, \frac{1}{2}(\tilde{\mathbf{u}}_{1h}^{n+1} + \mathbf{u}_h^n)) - (\mathbf{u}^*\phi_1^*, \frac{1}{2}\nabla(\mu_{11h}^{n+1} + \mu_{1h}^n)) + (\phi_1^*\nabla\mu_1^*, \frac{1}{2}(\tilde{\mathbf{u}}_{1h}^{n+1} + \mathbf{u}_h^n)) \\ \qquad - (\mathbf{u}^*\phi_2^*, \frac{1}{2}\nabla(\mu_{21h}^{n+1} + \mu_{2h}^n)) + (\phi_2^*\nabla\mu_2^*, \frac{1}{2}\nabla(\mu_{11h}^{n+1} + \mu_{1h}^n)) \\ \qquad + \lambda(H_1^*U^*, \frac{\phi_{11h}^{n+1} - \phi_{1h}^n}{\delta t}) - \lambda(H_1^*\phi_{1t}^*, \frac{1}{2}(U_{1h}^{n+1} + U_h^n)) \\ \qquad + \lambda(H_2^*U^*, \frac{\phi_{21h}^{n+1} - \phi_{2h}^n}{\delta t}) - \lambda(H_2^*\phi_{2t}^*, \frac{1}{2}(U_{1h}^{n+1} + U_h^n)), \\ \eta_2 = ((\mathbf{u}^*\cdot\nabla)\mathbf{u}^*, \frac{1}{2}\tilde{\mathbf{u}}_{2h}^{n+1}) - (\mathbf{u}^*\phi_1^*, \frac{1}{2}\nabla\mu_{12h}^{n+1}) + (\phi_1^*\nabla\mu_1^*, \frac{1}{2}\tilde{\mathbf{u}}_{2h}^{n+1}) - (\mathbf{u}^*\phi_2^*, \frac{1}{2}\nabla\mu_{22h}^{n+1}) + (\phi_2^*\nabla\mu_2^*, \frac{1}{2}\tilde{\mathbf{u}}_{2h}^{n+1}) \\ \qquad + \lambda(H_1^*U^*, \frac{\phi_{12h}^{n+1}}{\delta t}) - \lambda(H_1^*\phi_{1t}^*, \frac{1}{2}U_{2h}^{n+1}) + \lambda(H_2^*U^*, \frac{\phi_{22h}^{n+1}}{\delta t}) - \lambda(H_2^*\phi_{2t}^*, \frac{1}{2}U_{2h}^{n+1}). \end{cases} \tag{3.44}$$

It is very easy to solve (3.43) since all terms contained in η_1 and η_2 are already obtained from Steps 1, 2, and 3 (solvability of (3.43) is given below). Once $\bar{Q}^{n+\frac{1}{2}}$ is obtained from (3.43), we can update $\tilde{\mathbf{u}}^{n+1}$, ϕ_1^{n+1}, μ_1^{n+1}, ϕ_2^{n+1}, μ_2^{n+1} and U^{n+1} from (3.28), (3.37), and (3.40).

Now we further prove the solvability of (3.43) by showing $\frac{2}{\delta t} - \eta_2 \neq 0$. By setting $\boldsymbol{v}_h = \frac{1}{2}\tilde{\mathbf{u}}_{2h}^{n+1}$ in (3.42), we deduce

$$-((\mathbf{u}^*\cdot\nabla)\mathbf{u}^*, \frac{1}{2}\tilde{\mathbf{u}}_{2h}^{n+1}) - (\phi_1^*\nabla\mu_1^*, \frac{1}{2}\tilde{\mathbf{u}}_{2h}^{n+1}) - (\phi_2^*\nabla\mu_2^*, \frac{1}{2}\tilde{\mathbf{u}}_{2h}^{n+1}) = \frac{1}{2\delta t}\|\tilde{\mathbf{u}}_{2h}^{n+1}\|^2 + \frac{1}{4}\nu\|\nabla\tilde{\mathbf{u}}_{2h}^{n+1}\|^2. \tag{3.45}$$

By setting $w_{1h} = \frac{1}{2}\mu_{12h}^{n+1}$, $\Theta_{1h} = -\frac{1}{2\delta t}\phi_{12h}^{n+1}$, $\xi_{1h} = \frac{\lambda}{2\delta t}\psi_{12h}^{n+1}$ in (3.30), $\chi_{1h} = \frac{\lambda}{4\delta t}\Psi_{22h}^{n+1}$ in (3.32), and combining the four obtained equations, we get

$$(\mathbf{u}^*\phi_1^*, \frac{1}{2}\nabla\mu_{12h}^{n+1}) - \lambda(H_1^*U^*, \frac{\phi_{12h}^{n+1}}{\delta t}) = \frac{1}{4}M\|\nabla\mu_{12h}^{n+1}\|^2 + \frac{\lambda S}{2\delta t}\|\phi_{12h}^{n+1}\|^2 + \frac{\lambda}{2\delta t}\|\psi_{12h}^{n+1}\|^2 + \frac{\lambda}{4\delta t}(\Psi_{12h}^{n+1}, \Psi_{22h}^{n+1}). \tag{3.46}$$

By setting $w_{2h} = \frac{1}{2}\mu_{22h}^{n+1}$, $\Theta_{2h} = -\frac{1}{2\delta t}\phi_{22h}^{n+1}$, $\xi_{2h} = \frac{\lambda}{2\delta t}\psi_{22h}^{n+1}$ in (3.32), $\chi_{2h} = \frac{\lambda}{4\delta t}\Psi_{12h}^{n+1}$ in (3.30), and combining the four obtained equations, we get

$$(\mathbf{u}^*\phi_2^*, \frac{1}{2}\nabla\mu_{22h}^{n+1}) - \lambda(H_2^*U^*, \frac{\phi_{22h}^{n+1}}{\delta t}) = \frac{1}{4}M\|\nabla\mu_{22h}^{n+1}\|^2 + \frac{\lambda S}{2\delta t}\|\phi_{22h}^{n+1}\|^2 + \frac{\lambda}{2\delta t}\|\psi_{22h}^{n+1}\|^2 + \frac{\lambda}{4\delta t}(\Psi_{22h}^{n+1}, \Psi_{12h}^{n+1}). \tag{3.47}$$

By setting $V_h = \lambda U_{2h}^{n+1}$ in (3.39), we deduce

$$\lambda(H_1^*\phi_{1t}^*, \frac{1}{2}U_{2h}^{n+1}) + \lambda(H_2^*\phi_{2t}^*, \frac{1}{2}U_{2h}^{n+1}) = \frac{\lambda}{\delta t}\|U_{2h}^{n+1}\|^2. \tag{3.48}$$

Combining (3.45)-(3.48), we deduce

$$-\eta_2 = \frac{1}{2\delta t}\|\tilde{\mathbf{u}}_{2h}^{n+1}\|^2 + \frac{1}{4}\nu\|\nabla\tilde{\mathbf{u}}_{2h}^{n+1}\|^2 + \frac{1}{4}M\|\nabla\mu_{12h}^{n+1}\|^2 + \frac{1}{4}M\|\nabla\mu_{22h}^{n+1}\|^2 + \frac{\lambda}{\delta t}\|U_{2h}^{n+1}\|^2 + \frac{\lambda}{2\delta t}\left(S\|\phi_{12h}^{n+1}\|^2 + S\|\phi_{22h}^{n+1}\|^2 + \|\psi_{12h}^{n+1}\|^2 + \|\psi_{22h}^{n+1}\|^2 + (\Psi_{12h}^{n+1}, \Psi_{22h}^{n+1})\right). \tag{3.49}$$

From Lemma 3.1, assuming S satisfies the condition (2.65), we obtain $-\eta_2 \geq 0$. Thus (3.43) is always solvable.

Lemma 3.1. *If the constant S satisfies the condition (2.65), then the following inequality holds*

$$S\|\phi_{12h}^{n+1}\|^2 + S\|\phi_{22h}^{n+1}\|^2 + \|\psi_{12h}^{n+1}\|^2 + \|\psi_{22h}^{n+1}\|^2 + (\Psi_{12h}^{n+1}, \Psi_{22h}^{n+1}) \geq 0. \tag{3.50}$$

Proof. From (3.30), (3.32), and the definitions of $L_{12}^{\frac{1}{2}}$ in (3.13), we deduce

$$(\Psi_{12h}^{n+1} - \psi_{12h}^{n+1}, \xi_h) = a_{12}(\phi_{12h}^{n+1}, \xi_h), \quad (\Psi_{22h}^{n+1} - \psi_{22h}^{n+1}, \xi_h) = a_{12}(\phi_{22h}^{n+1}, \xi_h), \forall \xi_h \in Y_h. \tag{3.51}$$

By using a process similar to Lemma 2.1 or Lemma 2.4, we estimate $(\Psi_{12h}^{n+1}, \Psi_{22h}^{n+1})$ as

$$\begin{aligned}(\Psi_{12h}^{n+1}, \Psi_{22h}^{n+1}) &= (\Psi_{12h}^{n+1} - \psi_{12h}^{n+1}, \Psi_{22h}^{n+1}) + (\psi_{12h}^{n+1}, \Psi_{22h}^{n+1}) \\ &= (\Psi_{12h}^{n+1} - \psi_{12h}^{n+1}, \Psi_{22h}^{n+1} - \psi_{22h}^{n+1}) + (\Psi_{12h}^{n+1} - \psi_{12h}^{n+1}, \psi_{22h}^{n+1}) + (\psi_{12h}^{n+1}, \Psi_{22h}^{n+1} - \psi_{22h}^{n+1}) + (\psi_{12h}^{n+1}, \psi_{22h}^{n+1}) \\ &= a_{12}^2(\phi_{12h}^{n+1}, \phi_{22h}^{n+1}) + a_{12}(\phi_{12h}^{n+1}, \psi_{22h}^{n+1}) + a_{12}(\psi_{12h}^{n+1}, \phi_{22h}^{n+1}) + (\psi_{12h}^{n+1}, \psi_{22h}^{n+1}) \\ &\geq -\frac{a_{12}^2}{2}(\|\phi_{12h}^{n+1}\|^2 + \|\phi_{22h}^{n+1}\|^2) - \frac{\zeta}{4}\|\psi_{22h}^{n+1}\|^2 - \frac{1}{\zeta}a_{12}^2\|\phi_{12h}^{n+1}\|^2 \\ &\quad - \frac{\zeta}{4}\|\psi_{12h}^{n+1}\|^2 - \frac{1}{\zeta}a_{12}^2\|\phi_{22h}^{n+1}\|^2 - \frac{1}{2}\|\psi_{12h}^{n+1}\|^2 - \frac{1}{2}\|\psi_{22h}^{n+1}\|^2.\end{aligned} \tag{3.52}$$

Hence, we deduce

$$\begin{aligned}&S\|\phi_{12h}^{n+1}\|^2 + S\|\phi_{22h}^{n+1}\|^2 + \|\psi_{12h}^{n+1}\|^2 + \|\psi_{22h}^{n+1}\|^2 + (\Psi_{12h}^{n+1}, \Psi_{22h}^{n+1}) \\ &\quad \geq (\frac{1}{2} - \frac{\zeta}{4})\|\psi_{12h}^{n+1}\|^2 + (\frac{1}{2} - \frac{\zeta}{4})\|\psi_{22h}^{n+1}\|^2 + \left(S - \frac{a_{12}^2}{2} - \frac{1}{\zeta}a_{12}^2\right)\|\phi_{12h}^{n+1}\|^2 + \left(S - \frac{a_{12}^2}{2} - \frac{1}{\zeta}a_{12}^2\right)\|\phi_{22h}^{n+1}\|^2.\end{aligned} \tag{3.53}$$

Therefore, as long as the condition (2.65) is satisfied, we deduce (3.50), where we choose $\zeta = 1$ in (3.53). □

Step 5: we update $\mathbf{u}_h^{n+1}$ and p_h^{n+1} from (3.23) and (3.24).

As seen from the above implementation process, the computation process of the developed scheme is completely decoupled for all variables, and all nonlinear terms will not bring any variable coefficients, which means very efficient practical calculations.

3.3. Energy stability

In this subsection, we show that the fully discrete scheme (3.14)-(3.24) is unconditionally energy stable. We will use the following two identities repeatedly:

$$2(a-b)a = |a|^2 - |b|^2 + |a-b|^2, \tag{3.54}$$

$$(a-b, 3b-c) = \left(|a|^2 - \frac{1}{2}|a-b|^2\right) - \left(|b|^2 - \frac{1}{2}|b-c|^2\right) - \frac{1}{2}|a-2b+c|^2. \tag{3.55}$$

Theorem 3.1. *When S satisfies the condition (2.65), the fully-discrete scheme (3.14)-(3.24) follows the following discrete energy dissipation law:*

$$\frac{1}{\delta t}(E_h^{n+1} - E_h^n) = -\nu\|\nabla\bar{\mathbf{u}}_h^{n+\frac{1}{2}}\|^2 - M\|\nabla\bar{\mu}_{1h}^{n+\frac{1}{2}}\|^2 - M\|\nabla\bar{\mu}_{2h}^{n+\frac{1}{2}}\|^2 \leq 0, \tag{3.56}$$

where E_h^{n+1} is bounded from below and defined as

$$
\begin{aligned}
E_h^{n+1} =& \frac{1}{2}\|\mathbf{u}_h^{n+1}\|^2 + \lambda\frac{1}{2}\Big\{\|\psi_{1h}^{n+1}\|^2 + \|\psi_{2h}^{n+1}\|^2 + (\Psi_{1h}^{n+1}, \Psi_{2h}^{n+1}) \\
&- 2a_1\|\nabla\phi_{1h}^{n+1}\|^2 - 2a_2\|\nabla\phi_{2h}^{n+1}\|^2 + S\|\phi_{1h}^{n+1}\|^2 + S\|\phi_{2h}^{n+1}\|^2\Big\} \\
&+ \frac{\lambda}{2}a_1\|\nabla\phi_{1h}^{n+1} - \nabla\phi_{1h}^{n}\|^2 + \frac{\lambda}{2}a_2\|\nabla\phi_{2h}^{n+1} - \nabla\phi_{2h}^{n}\|^2 + \lambda\|U^{n+1}\|^2 + \frac{1}{2}|Q^{n+1}|^2 \\
&+ \frac{\delta t^2}{8}\|\nabla p_h^{n+1}\|^2 - \frac{1}{2} - B|\Omega|.
\end{aligned} \tag{3.57}
$$

Proof. We now prove the dissipative law (3.56) as follows. The property of boundedness (from below) of the discrete energy E_h^{n+1} will be shown in Theorem 3.2.

Taking $\boldsymbol{v}_h = 2\delta t\bar{\tilde{\mathbf{u}}}_h^{n+\frac{1}{2}} = \delta t(\tilde{\mathbf{u}}_h^{n+1} + \mathbf{u}_h^n)$ in (3.22), and using (3.54) and integration by parts, we obtain

$$
\begin{aligned}
&\|\tilde{\mathbf{u}}_h^{n+1}\|^2 - \|\mathbf{u}_h^n\|^2 + 2\nu\delta t\|\nabla\bar{\tilde{\mathbf{u}}}_h^{n+\frac{1}{2}}\|^2 + 2\delta t(\nabla p_h^n, \bar{\tilde{\mathbf{u}}}_h^{n+\frac{1}{2}}) \\
&+ 2\delta t\bar{Q}^{n+\frac{1}{2}}((\mathbf{u}^*\cdot\nabla)\mathbf{u}^*, \bar{\tilde{\mathbf{u}}}_h^{n+\frac{1}{2}}) + 2\delta t\bar{Q}^{n+\frac{1}{2}}(\phi_1^*\nabla\mu_1^*, \bar{\tilde{\mathbf{u}}}_h^{n+\frac{1}{2}}) + 2\delta t\bar{Q}^{n+\frac{1}{2}}(\phi_2^*\nabla\mu_2^*, \bar{\tilde{\mathbf{u}}}_h^{n+\frac{1}{2}}) = 0.
\end{aligned} \tag{3.58}
$$

We rewrite (3.24) as

$$
\mathbf{u}_h^{n+1} - \tilde{\mathbf{u}}_h^{n+1} = -\frac{\delta t}{2}\nabla(p_h^{n+1} - p_h^n). \tag{3.59}
$$

Taking the L^2 inner product for the above equation with $\mathbf{u}_h^{n+1}$ and using (3.27), we derive

$$
\|\mathbf{u}_h^{n+1}\|^2 - \|\tilde{\mathbf{u}}_h^{n+1}\|^2 + \|\mathbf{u}_h^{n+1} - \tilde{\mathbf{u}}_h^{n+1}\|^2 = 0. \tag{3.60}
$$

We further rewrite (3.24) as

$$
\mathbf{u}_h^{n+1} + \mathbf{u}_h^n + \frac{\delta t}{2}(\nabla p_h^{n+1} - \nabla p_h^n) = 2\bar{\tilde{\mathbf{u}}}_h^{n+\frac{1}{2}}.
$$

Taking the L^2 inner product for the above equation $\delta t\nabla p_h^n$ and using (3.27), we derive

$$
2\delta t(\bar{\tilde{\mathbf{u}}}_h^{n+\frac{1}{2}}, \nabla p_h^n) = \frac{\delta t^2}{4}(\|\nabla p_h^{n+1}\|^2 - \|\nabla p_h^n\|^2) - \frac{\delta t^2}{4}\|\nabla p_h^{n+1} - \nabla p_h^n\|^2. \tag{3.61}
$$

By taking the square of (3.59), we deduce

$$
-\|\mathbf{u}_h^{n+1} - \tilde{\mathbf{u}}_h^{n+1}\|^2 = -\frac{\delta t^2}{4}\|\nabla p_h^{n+1} - \nabla p_h^n\|^2. \tag{3.62}
$$

By combining (3.58), (3.60), (3.61) and (3.62), we derive

$$
\begin{aligned}
&\|\mathbf{u}_h^{n+1}\|^2 - \|\mathbf{u}_h^n\|^2 + \frac{\delta t^2}{4}(\|\nabla p_h^{n+1}\|^2 - \|\nabla p_h^n\|^2) = -2\nu\delta t\|\nabla\bar{\tilde{\mathbf{u}}}_h^{n+\frac{1}{2}}\|^2 \\
&\underbrace{-2\delta t\bar{Q}^{n+\frac{1}{2}}((\mathbf{u}^*\cdot\nabla)\mathbf{u}^*, \bar{\tilde{\mathbf{u}}}_h^{n+\frac{1}{2}})}_{I_1}\underbrace{-2\delta t\bar{Q}^{n+\frac{1}{2}}(\phi_1^*\nabla\mu_1^*, \bar{\tilde{\mathbf{u}}}_h^{n+\frac{1}{2}})}_{II_1}\underbrace{-2\delta t\bar{Q}^{n+\frac{1}{2}}(\phi_2^*\nabla\mu_2^*, \bar{\tilde{\mathbf{u}}}_h^{n+\frac{1}{2}})}_{III_1}.
\end{aligned} \tag{3.63}
$$

Taking $w_{1h} = 2\delta t\bar{\mu}_{1h}^{n+\frac{1}{2}}$ in (3.14), we derive

$$
2(\phi_{1h}^{n+1} - \phi_{1h}^n, \bar{\mu}_{1h}^{n+\frac{1}{2}}) = -2\delta tM\|\nabla\bar{\mu}_{1h}^{n+\frac{1}{2}}\|^2\underbrace{+2\delta t\bar{Q}^{n+\frac{1}{2}}(\mathbf{u}^*\phi_1^*, \nabla\bar{\mu}_{1h}^{n+\frac{1}{2}})}_{IV_1}. \tag{3.64}
$$

Taking $\Theta_{1h} = -2(\phi_{1h}^{n+1} - \phi_{1h}^n)$ in (3.15), we find

$$
\begin{aligned}
-2(\bar{\mu}_{1h}^{n+\frac{1}{2}}, \phi_{1h}^{n+1} - \phi_{1h}^n) =& 2\lambda(\nabla\bar{\psi}_{1h}^{n+\frac{1}{2}}, \nabla(\phi_{1h}^{n+1} - \phi_{1h}^n)) - 4\lambda a_1(\psi_1^*, \phi_{1h}^{n+1} - \phi_{1h}^n) \\
&- \lambda(L_{12}^{\frac{1}{2}}\bar{\Psi}_{2h}^{n+\frac{1}{2}}, L_{12}^{\frac{1}{2}}(\phi_{1h}^{n+1} - \phi_{1h}^n)) - 2\lambda S(\bar{\phi}_{1h}^{n+\frac{1}{2}}, \phi_{1h}^{n+1} - \phi_{1h}^n) \\
&\underbrace{-2\lambda\bar{Q}^{n+\frac{1}{2}}(H_1^*U^*, \phi_{1h}^{n+1} - \phi_{1h}^n)}_{V_1}.
\end{aligned} \tag{3.65}
$$

Taking $w_{2h}=2\delta t\bar{\mu}_{2h}^{n+\frac{1}{2}}$ in (3.16), we derive

$$2(\phi_{2h}^{n+1}-\phi_{2h}^{n},\bar{\mu}_{2h}^{n+\frac{1}{2}})=-2\delta tM\|\nabla\bar{\mu}_{2h}^{n+\frac{1}{2}}\|^2\underbrace{+2\delta t\bar{Q}^{n+\frac{1}{2}}(\mathbf{u}^*\phi_2^*,\nabla\bar{\mu}_{2h}^{n+\frac{1}{2}})}_{VI_1}. \tag{3.66}$$

Taking $\Theta_{2h}=-2(\phi_{2h}^{n+1}-\phi_{2h}^{n})$ in (3.17), we find

$$\begin{aligned}-2(\bar{\mu}_{2h}^{n+\frac{1}{2}},\phi_{2h}^{n+1}-\phi_{2h}^{n})&=2\lambda(\nabla\bar{\psi}_{2h}^{n+\frac{1}{2}},\nabla(\phi_{2h}^{n+1}-\phi_{2h}^{n}))-4\lambda a_2(\psi_2^*,\phi_{2h}^{n+1}-\phi_{2h}^{n})\\&-\lambda(L_{12}^{\frac{1}{2}}\bar{\Psi}_{1h}^{n+\frac{1}{2}},L_{12}^{\frac{1}{2}}(\phi_{2h}^{n+1}-\phi_{2h}^{n}))-2\lambda S(\bar{\phi}_{2h}^{n+\frac{1}{2}},\phi_{2h}^{n+1}-\phi_{2h}^{n})\underbrace{-2\lambda\bar{Q}^{n+\frac{1}{2}}(H_2^*U^*,\phi_{2h}^{n+1}-\phi_{2h}^{n})}_{VII_1}.\end{aligned} \tag{3.67}$$

We apply the two equations in (3.18) to two consecutive time nodes at t^n,t^{n-1} to get

$$\begin{cases}(3\psi_{1h}^{n}-\psi_{1h}^{n-1},\xi_{1h})=2(\psi_1^*,\xi_{1h})=-(\nabla(3\phi_{1h}^{n}-\phi_{1h}^{n-1}),\nabla\xi_{1h}),\\(3\psi_{2h}^{n}-\psi_{2h}^{n-1},\xi_{2h})=2(\psi_2^*,\xi_{2h})=-(\nabla(3\phi_{2h}^{n}-\phi_{2h}^{n-1}),\nabla\xi_{2h}).\end{cases} \tag{3.68}$$

Taking $\xi_{1h}=-2\lambda a_1(\phi_{1h}^{n+1}-\phi_{1h}^{n})$, $\xi_{2h}=-2\lambda a_2(\phi_{2h}^{n+1}-\phi_{2h}^{n})$ in (3.68), we get

$$\begin{aligned}-4\lambda a_1(\psi_1^*,\phi_{1h}^{n+1}-\phi_{1h}^{n})&=2\lambda a_1(\nabla(3\phi_{1h}^{n}-\phi_{1h}^{n-1}),\nabla\phi_{1h}^{n+1}-\nabla\phi_{1h}^{n})\\&=2\lambda a_1(\|\nabla\phi_{1h}^{n+1}\|^2-\frac{1}{2}\|\nabla\phi_{1h}^{n+1}-\nabla\phi_{1h}^{n}\|^2)\\&-2\lambda a_1(\|\nabla\phi_{1h}^{n}\|^2-\frac{1}{2}\|\nabla\phi_{1h}^{n}-\nabla\phi_{1h}^{n-1}\|^2)-2\lambda a_1\frac{1}{2}\|\nabla\phi_{1h}^{n+1}-2\nabla\phi_{1h}^{n}+\nabla\phi_{1h}^{n-1}\|^2,\\-4\lambda a_2(\psi_2^*,\phi_{2h}^{n+1}-\phi_{2h}^{n})&=2\lambda a_2(\nabla(3\phi_{2h}^{n}-\phi_{2h}^{n-1}),\nabla\phi_{2h}^{n+1}-\nabla\phi_{2h}^{n})\\&=2\lambda a_2(\|\nabla\phi_{2h}^{n+1}\|^2-\frac{1}{2}\|\nabla\phi_{2h}^{n+1}-\nabla\phi_{2h}^{n}\|^2)\\&-2\lambda a_2(\|\nabla\phi_{2h}^{n}\|^2-\frac{1}{2}\|\nabla\phi_{2h}^{n}-\nabla\phi_{2h}^{n-1}\|^2)-2\lambda a_1\frac{1}{2}\|\nabla\phi_{2h}^{n+1}-2\nabla\phi_{2h}^{n}+\nabla\phi_{2h}^{n-1}\|^2.\end{aligned}$$

We apply the four equations in (3.18) and (3.19) to two consecutive time nodes at t^{n+1},t^n to obtain

$$\begin{cases}(\psi_{1h}^{n+1}-\psi_{1h}^{n},\xi_{1h})=-(\nabla(\phi_{1h}^{n+1}-\phi_{1h}^{n}),\nabla\xi_{1h}),\ (\psi_{2h}^{n+1}-\psi_{2h}^{n},\xi_{2h})=-(\nabla(\phi_{2h}^{n+1}-\phi_{2h}^{n}),\nabla\xi_{2h}),\\(\Psi_{1h}^{n+1}-\Psi_{1h}^{n},\chi_{1h})=(L_{12}^{\frac{1}{2}}(\phi_{1h}^{n+1}-\phi_{1h}^{n}),L_{12}^{\frac{1}{2}}\chi_{1h}),\ (\Psi_{2h}^{n+1}-\Psi_{2h}^{n},\chi_{2h})=(L_{12}^{\frac{1}{2}}(\phi_{2h}^{n+1}-\phi_{2h}^{n}),L_{12}^{\frac{1}{2}}\chi_{2h}).\end{cases} \tag{3.69}$$

Taking $\xi_{1h}=2\lambda\bar{\psi}_{1h}^{n+\frac{1}{2}}$, $\xi_{2h}=2\lambda\bar{\psi}_{2h}^{n+\frac{1}{2}}$, $\chi_{1h}=\lambda\bar{\Psi}_{2h}^{n+\frac{1}{2}}$, $\chi_{2h}=\lambda\bar{\Psi}_{1h}^{n+\frac{1}{2}}$ in (3.69), we get

$$\begin{cases}2\lambda(\psi_{1h}^{n+1}-\psi_{1h}^{n},\bar{\psi}_{1h}^{n+\frac{1}{2}})=\lambda(\|\psi_{1h}^{n+1}\|^2-\|\psi_{1h}^{n}\|^2)=-2\lambda(\nabla(\phi_{1h}^{n+1}-\phi_{1h}^{n}),\nabla\bar{\psi}_{1h}^{n+\frac{1}{2}}),\\2\lambda(\psi_{2h}^{n+1}-\psi_{2h}^{n},\bar{\psi}_{2h}^{n+\frac{1}{2}})=\lambda(\|\psi_{2h}^{n+1}\|^2-\|\psi_{2h}^{n}\|^2)=-2\lambda(\nabla(\phi_{2h}^{n+1}-\phi_{2h}^{n}),\nabla\bar{\psi}_{2h}^{n+\frac{1}{2}}),\\\lambda(\Psi_{1h}^{n+1}-\Psi_{1h}^{n},\bar{\Psi}_{2h}^{n+\frac{1}{2}})=\lambda(L_{12}^{\frac{1}{2}}(\phi_{1h}^{n+1}-\phi_{1h}^{n}),L_{12}^{\frac{1}{2}}\bar{\Psi}_{2h}^{n+\frac{1}{2}}),\\\lambda(\Psi_{2h}^{n+1}-\Psi_{2h}^{n},\bar{\Psi}_{1h}^{n+\frac{1}{2}})=\lambda(L_{12}^{\frac{1}{2}}(\phi_{2h}^{n+1}-\phi_{2h}^{n}),L_{12}^{\frac{1}{2}}\bar{\Psi}_{1h}^{n+\frac{1}{2}}).\end{cases} \tag{3.70}$$

Taking $V_h=4\lambda\delta t\bar{U}_h^{n+\frac{1}{2}}$ in (3.20), we obtain

$$4\lambda(U_h^{n+1}-U_h^{n},\bar{U}_h^{n+\frac{1}{2}})=\underbrace{2\delta t\lambda\bar{Q}^{n+\frac{1}{2}}(H_1^*\phi_{1t}^*,\bar{U}_h^{n+\frac{1}{2}})}_{VIII_1}+\underbrace{2\delta t\lambda\bar{Q}^{n+\frac{1}{2}}(H_2^*\phi_{2t}^*,\bar{U}_h^{n+\frac{1}{2}})}_{IX_1}. \tag{3.71}$$

By multiplying (3.21) with $2\delta t\bar{Q}^{n+\frac{1}{2}}$ and using (3.54), we obtain

$$\begin{aligned}&2(Q^{n+1}-Q^{n})\bar{Q}^{n+\frac{1}{2}}\\&=\underbrace{2\delta t\bar{Q}^{n+\frac{1}{2}}((\mathbf{u}^*\cdot\nabla)\mathbf{u}^*,\bar{\tilde{\mathbf{u}}}_h^{n+\frac{1}{2}})}_{I_2}\underbrace{-2\delta t\bar{Q}^{n+\frac{1}{2}}(\mathbf{u}^*\phi_1^*,\nabla\bar{\mu}_{1h}^{n+\frac{1}{2}})}_{IV_2}+\underbrace{2\delta t\bar{Q}^{n+\frac{1}{2}}(\phi_1^*\nabla\mu_1^*,\bar{\tilde{\mathbf{u}}}_h^{n+\frac{1}{2}})}_{II_2}\end{aligned} \tag{3.72}$$

$$\underbrace{-2\delta t\bar{Q}^{n+\frac{1}{2}}(\mathbf{u}^*\phi_2^*,\nabla\bar{\mu}_{2h}^{n+\frac{1}{2}})}_{VI_2}+\underbrace{2\delta t\bar{Q}^{n+\frac{1}{2}}(\phi_2^*\nabla\mu_2^*,\tilde{\mathbf{u}}_h^{n+\frac{1}{2}})}_{III_2}\underbrace{+2\lambda\bar{Q}^{n+\frac{1}{2}}(H_1^*U^*,\phi_{1h}^{n+1}-\phi_{1h}^n)}_{V_2}$$
$$\underbrace{-2\delta t\lambda\bar{Q}^{n+\frac{1}{2}}(H_1^*\phi_{1t}^*,\bar{U}^{n+\frac{1}{2}})}_{VIII_2}\underbrace{+2\lambda\bar{Q}^{n+\frac{1}{2}}(H_2^*U^*,\phi_{2h}^{n+1}-\phi_{2h}^n)}_{VII_2}\underbrace{-2\delta t\lambda\bar{Q}^{n+\frac{1}{2}}(H_2^*\phi_{2t}^*,\bar{U}^{n+\frac{1}{2}})}_{IX_2}. \tag{3.73}$$

Hence, by combining (3.63), (3.64), (3.65), (3.70)-(3.72), using (3.54), and noticing that all under braced terms with the same Roman numerals are canceled, we arrive at

$$\begin{aligned}
&\|\mathbf{u}_h^{n+1}\|^2-\|\mathbf{u}_h^n\|^2+\frac{\delta t^2}{4}(\|\nabla p_h^{n+1}\|^2-\|\nabla p_h^n\|^2)\\
&\quad+\lambda(\|\psi_{1h}^{n+1}\|^2-\|\psi_{1h}^n\|^2)+\lambda(\|\psi_{2h}^{n+1}\|^2-\|\psi_{2h}^n\|^2)+\lambda(\Psi_{1h}^{n+1},\Psi_{2h}^{n+1})-\lambda(\Psi_{1h}^n,\Psi_{2h}^n)\\
&\quad-2\lambda a_1(\|\nabla\phi_{1h}^{n+1}\|^2-\frac{1}{2}\|\nabla\phi_{1h}^{n+1}-\nabla\phi_{1h}^n\|^2)+2\lambda a_1(\|\nabla\phi_{1h}^n\|^2-\frac{1}{2}\|\nabla\phi_{1h}^n-\nabla\phi_{1h}^{n-1}\|^2)\\
&\quad-2\lambda a_2(\|\nabla\phi_{2h}^{n+1}\|^2-\frac{1}{2}\|\nabla\phi_{2h}^{n+1}-\nabla\phi_{2h}^n\|^2)+2\lambda a_2(\|\nabla\phi_{2h}^n\|^2-\frac{1}{2}\|\nabla\phi_{2h}^n-\nabla\phi_{2h}^{n-1}\|^2)\\
&\quad+\lambda S(\|\phi_{1h}^{n+1}\|^2-\|\phi_{1h}^n\|^2)+\lambda S(\|\phi_{2h}^{n+1}\|^2-\|\phi_{2h}^n\|^2)+2\lambda(\|U_h^{n+1}\|^2-\|U_h^n\|^2)\\
&\quad+(|Q^{n+1}|^2-|Q^n|^2)=-2\delta t\nu\|\nabla\tilde{\mathbf{u}}_h^{n+\frac{1}{2}}\|^2-2\delta tM\|\nabla\bar{\mu}_{1h}^{n+\frac{1}{2}}\|^2-2\delta tM\|\nabla\bar{\mu}_{2h}^{n+\frac{1}{2}}\|^2.
\end{aligned}\tag{3.74}$$

Finally, by dividing 2 of (3.74) and dropping some unnecessary positive terms, we obtain (3.56). □

Theorem 3.2. *If the constant S satisfies the condition (2.65), then the discrete energy E_h^{n+1} given in (3.57) is bounded from below.*

Proof. From the definitions of $L_{12}^{\frac{1}{2}}$ in (3.13) and (3.18)-(3.19), we deduce

$$\begin{aligned}
&(\Psi_{1h}^{n+1}-\psi_{1h}^{n+1},\xi_h)=a_{12}(\phi_{1h}^{n+1},\xi_h),\\
&(\Psi_{2h}^{n+1}-\psi_{2h}^{n+1},\xi_h)=a_{12}(\phi_{2h}^{n+1},\xi_h),\forall\xi_h\in Y_h.
\end{aligned}\tag{3.75}$$

Using the Cauchy-Schwarz inequality, we estimate $(\Psi_{1h}^{n+1},\Psi_{2h}^{n+1})$ as

$$\begin{aligned}
(\Psi_{1h}^{n+1},\Psi_{2h}^{n+1})&=(\Psi_{1h}^{n+1}-\psi_{1h}^{n+1},\Psi_{2h}^{n+1})+(\psi_{1h}^{n+1},\Psi_{2h}^{n+1})\\
&=(\Psi_{1h}^{n+1}-\psi_{1h}^{n+1},\Psi_{2h}^{n+1}-\psi_{2h}^{n+1})+(\Psi_{1h}^{n+1}-\psi_{1h}^{n+1},\psi_{2h}^{n+1})\\
&\quad+(\psi_{1h}^{n+1},\Psi_{2h}^{n+1}-\psi_{2h}^{n+1})+(\psi_{1h}^{n+1},\psi_{2h}^{n+1})\\
&=a_{12}^2(\phi_{1h}^{n+1},\phi_{2h}^{n+1})+a_{12}(\phi_{1h}^{n+1},\psi_{2h}^{n+1})+a_{12}(\psi_{1h}^{n+1},\phi_{2h}^{n+1})+(\psi_{1h}^{n+1},\psi_{2h}^{n+1})\\
&\geq-\frac{a_{12}^2}{2}(\|\phi_{1h}^{n+1}\|^2+\|\phi_{2h}^{n+1}\|^2)-\frac{\zeta}{4}\|\psi_{2h}^{n+1}\|^2-\frac{1}{\zeta}a_{12}^2\|\phi_{1h}^{n+1}\|^2\\
&\quad-\frac{\zeta}{4}\|\psi_{1h}^{n+1}\|^2-\frac{1}{\zeta}a_{12}^2\|\phi_{2h}^{n+1}\|^2-\frac{1}{2}\|\psi_{1h}^{n+1}\|^2-\frac{1}{2}\|\psi_{2h}^{n+1}\|^2.
\end{aligned}\tag{3.76}$$

Second, we estimate the negative terms $-a_1\|\nabla\phi_{1h}^{n+1}\|^2-a_2\|\nabla\phi_{2h}^{n+1}\|^2$ as follows

$$\begin{aligned}
-2a_1\|\nabla\phi_{1h}^{n+1}\|^2-2a_2\|\nabla\phi_{2h}^{n+1}\|^2&=-2a_1(\nabla\phi_{1h}^{n+1},\nabla\phi_{1h}^{n+1})-2a_2(\nabla\phi_{2h}^{n+1},\nabla\phi_{2h}^{n+1})\\
&=2a_1(\psi_{1h}^{n+1},\phi_{1h}^{n+1})+2a_2(\psi_{2h}^{n+1},\phi_{2h}^{n+1})\\
&\geq-\frac{\eta}{4}\|\psi_{1h}^{n+1}\|^2-\frac{4}{\eta}a_1^2\|\phi_{1h}^{n+1}\|^2-\frac{\eta}{4}\|\psi_{2h}^{n+1}\|^2-\frac{4}{\eta}a_2^2\|\phi_{2h}^{n+1}\|^2,
\end{aligned}\tag{3.77}$$

where we use (3.18) and the Cauchy-Schwarz inequality.

Hence, we deduce

$$\begin{aligned}
&\|\psi_{1h}^{n+1}\|^2+\|\psi_{2h}^{n+1}\|^2+(\Psi_{1h}^{n+1},\Psi_{2h}^{n+1})-a_1\|\nabla\phi_{1h}^{n+1}\|^2-a_2\|\nabla\phi_{2h}^{n+1}\|^2+S\|\phi_{1h}^{n+1}\|^2+S\|\phi_{2h}^{n+1}\|^2\\
&\quad\geq(\frac{1}{2}-\frac{\zeta}{4}-\frac{\eta}{4})\|\psi_{1h}^{n+1}\|^2+(\frac{1}{2}-\frac{\zeta}{4}-\frac{\eta}{4})\|\psi_{2h}^{n+1}\|^2\\
&\quad\quad+\Big(S-\frac{a_{12}^2}{2}-\frac{1}{\zeta}a_{12}^2-\frac{4}{\eta}a_1^2\Big)\|\phi_{1h}^{n+1}\|^2+\Big(S-\frac{a_{12}^2}{2}-\frac{1}{\zeta}a_{12}^2-\frac{4}{\eta}a_2^2\Big)\|\phi_{2h}^{n+1}\|^2.
\end{aligned}\tag{3.78}$$

Therefore, as long as the condition (2.65) is satisfied, the energy E_h^{n+1} is bounded from below, where we choose $\zeta=\eta=1$ in (3.78). □

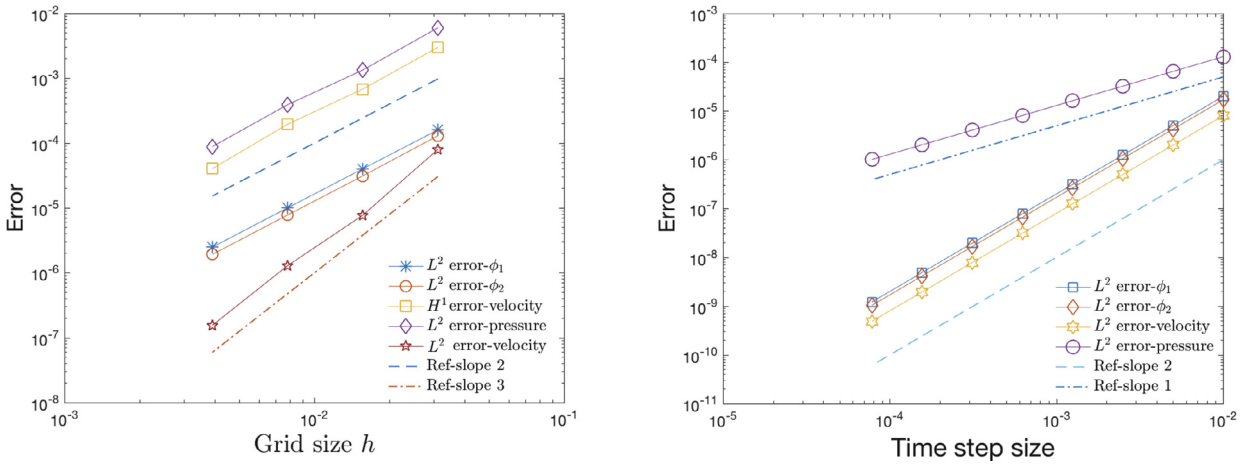

(a) Spatial error. (b) Temporal error.

Fig. 4.1. Convergence order tests for spatial and temporal discretization, where the numerical errors at $t = 1$ for all variables are computed. (For interpretation of the colors in the figure(s), the reader is referred to the web version of this article.)

4. Numerical simulations

In this section, the accuracy, energy stability of the proposed explicit-IEQ scheme (3.14)-(3.24) (denoted by EIEQ, for short) will be investigated. Various numerical tests will be carried out, including binary crystal growth affected by the imposed shear flow acting on the wall boundary and the sedimentation process of many particles of binary alloys under the action of gravity. We use Taylor-Hood elements [15] for $\boldsymbol{V}_h$ and O_h that satisfy inf-sup condition and set the finite element spaces (3.1) with $l_1 = 1, l_2 = 2, l_3 = 1$.

4.1. Accuracy and stability test

We first verify the convergence rate of the EIEQ scheme by conducting 2D simulations for the flow-coupled binary PFC model. The computational domain is set as $\Omega = [0, 2\pi]^2$. By setting some suitable forcing functions, we assume the exact solution of the system read as

$$\begin{cases} \phi_1(x, y, t) = \cos(2x)\cos(2y)\cos t, \quad \phi_2(x, y, t) = \cos(x)\cos(y)\cos t, \quad p(x, y, t) = \cos(x)\cos(y)\sin t, \\ \mathbf{u}(x, y, t) = (u(x, y, t), v(x, y, t)) = \cos(t)(\sin(2y)\sin^2(x), -\sin(2x)\sin^2(y)). \end{cases} \tag{4.1}$$

The boundary conditions are specified in (2.16), and the model parameters are set as $a_1 = a_2 = 1$, $a_{12} = 1.2$, $\varepsilon = 0.1$, $\nu = 1$, $S = 4$, $M = 1$, $\gamma = 0.5$, $\beta = 10$, $\lambda = 0.01$, $B = 1\text{e}5$.

In Fig. 4.1 (a), we first verify the spatial convergence order by plotting the error in various norms which are computed using various grid size h. We choose δt to be small enough ($\delta t = 1\text{e}{-5}$) so that the errors are dominated by the spatial discretization error. We can see that the second-order convergence rate is followed by the H^1-error for the velocity, L^2-error of the pressure p, and L^2-error of the two phase-field variables ϕ_1 and ϕ_2. The third-order convergence rate is observed for L^2 error of the velocity. These results fully agree with the theoretical expectation of accuracy for $P2/P1$ element of $(\mathbf{u}, p)$ and $P1$ element of ϕ_1 and ϕ_2.

In Fig. 4.1 (b), we verify the temporal convergence order by fixing the grid size $h = \frac{2\pi}{256}$. In this way, the spatial grid size is small enough and the spatial discretization errors are negligible compared with the time discretization error. The L^2-errors between the numerical solution of $\phi, \mathbf{u}, p$ and the exact solution at $t = 1$ are plotted, where various time step sizes from $\delta t = 0.01$ to $\delta t = 0.01/2^5$ (with factor of 2) are used. It can be observed that the scheme EIEQ gives the second-order time accuracy of $\mathbf{u}$ and ϕ, and the first-order time accuracy of p (note that the pressure is only first-order accurate for the particular projection type scheme used in this article due to the boundary layer phenomenon, see the theoretical/numerical evidence in [36,20,7,29,17]).

To further test the energy stability of the developed scheme, we use the well-known phase separation (spinodal decomposition) example of the vacancy PFC model (see also in [5]). The 2D computational domain is set as $\Omega = [0, 200]^2$, and the initial conditions read as follows:

$$\begin{aligned} &\phi_1^0(x, y) = 0.07 + 0.001\text{rand}(x, y), \quad \phi_2^0(x, y) = 0.07 + 0.001\text{rand}(x, y), \\ &\mathbf{u}^0(x, y) = \mathbf{0}, \, p^0(x, y) = 0, \end{aligned} \tag{4.2}$$

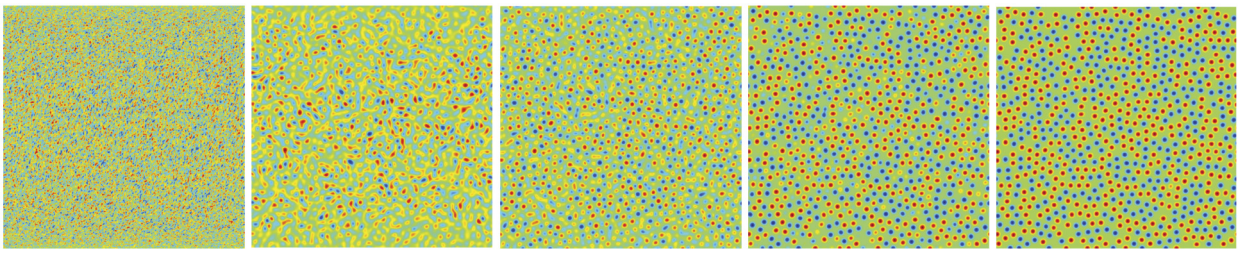

Fig. 4.2. Snapshots of $\phi_1 - \phi_2$ at $t = 0, 6, 13, 20$ and 75 for the phase separation example with the initial conditions given in (4.2).

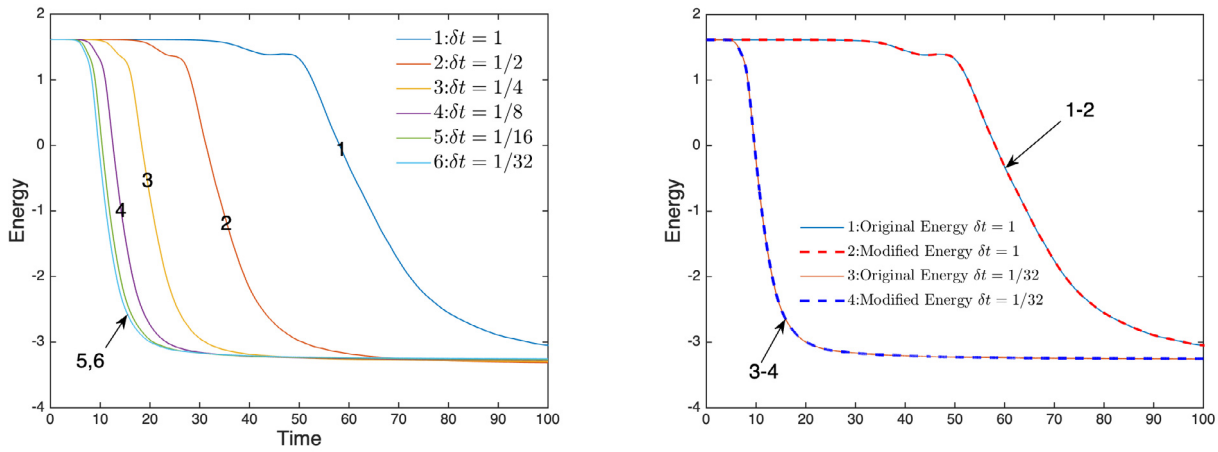

(a) Free energy evolution computed by various time steps. (b) Energy comparisons: modified and original.

Fig. 4.3. (a) Time evolution of the free energy (2.18) computed by using various time step sizes; and (b) the energy evolutions of the free energy (2.18) (original form) and (3.57) (modified discrete form) computed by using the scheme EIEQ and two different time steps $\delta t = 1$ and $\frac{1}{32}$.

where rand(x, y) is the random number in the range $[-1, 1]$. The model parameters are set as $a_1 = a_2 = 1$, $a_{12} = 1.2$, $\varepsilon = 0.9$, $\nu = 1$, $S = 4$, $M = 1$, $\gamma = 0.5$, $\beta = 3000$, $\lambda = 0.01$, $B =$ 1e5, $\delta t = 0.01$, $h = \frac{200}{256}$. We plot the snapshots of the configuration profile $\phi_1 - \phi_2$ at different times in Fig. 4.2. We observe that the final steady state shows clusters of binary particles with vacancies in the entire region, which is qualitatively consistent with the simulations shown in [2,5].

Further numerical simulations are carried out to verify the time marching energy stability. The time evolution of the free energy (2.18) computed using various time steps (from $\delta t = 1$ to $\delta t = \frac{1}{32}$ with the factor $1/2$) are shown in Fig. 4.3 (a). We observe that all obtained energy curves show monotonic decays, thus verifying the unconditional stability of EIEQ. In Fig. 4.3 (b), we plot the time evolution of the free energy in the original form (2.18) and the discrete energy (3.57) using the time step size $\delta t = 1$ and $\delta t = \frac{1}{32}$. We find these two energies have almost invisible differences.

4.2. Crystal growth in a shear flow regime

In this example, for the no-vacancy model ($\beta = 0$), we study how the fluid flow affects the dynamical growth of binary crystal particles. We refer to [10,37,16,39] for single-phase crystal growth simulation, in which the model set does not involve the vacancy potential and flow field.

We carry out numerical simulations in 2D with the computed domain $[0, 512]^2$. The model parameters are set as $a_1 = a_2 = 1$, $a_{12} = 1.2$, $\varepsilon = 0.05$, $\nu = 1$, $S = 4$, $M = 1$, $\gamma = 0.1$, $\beta = 0$, $\lambda = 0.01$, $B =$ 1e5, $\delta t = 0.01$, $h = 1$. We set the boundary condition (2.16) along the y-direction and assume that the x-direction satisfies the periodic boundary condition.

We first simulate the no-flow situation (i.e., $\mathbf{u} = \mathbf{0}$, $p = 0$) to study how a small binary core gradually forms an ordered pattern to the entire domain. In order to obtain the initial configuration of one or more tiny crystal nuclei as seeds, we implement EIEQ for sufficiently long enough time and cut out a small circular patch from the designated area. See below for the detailed process of obtaining the initial conditions of $\phi_i^0(x, y), i = 1, 2$.

First, we define two functions $\Phi_i(x, y)$ $(i = 1, 2)$:

$$\Phi_i(x, y) = \begin{cases} \bar{\phi} + q\Big(\cos(\frac{\zeta}{\sqrt{3}} y_l^i)\cos(px_l^i) - 0.5\cos(\frac{2\zeta}{\sqrt{3}} y_l^i)\Big), & \text{if } (x_l^i, y_l^i) \in \mathscr{D}, \\ \bar{\phi}, & \text{else,} \end{cases} \tag{4.3}$$

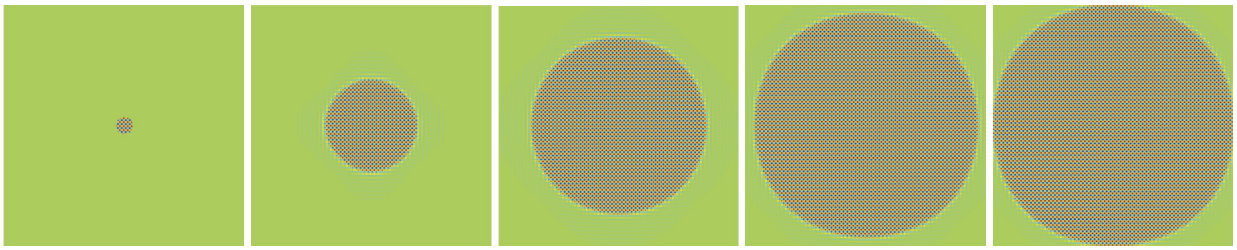

(a) No flow case, snapshots of $\phi_1 - \phi_2$ are taken at $t = 0, 500, 1000, 1500, 1700$.

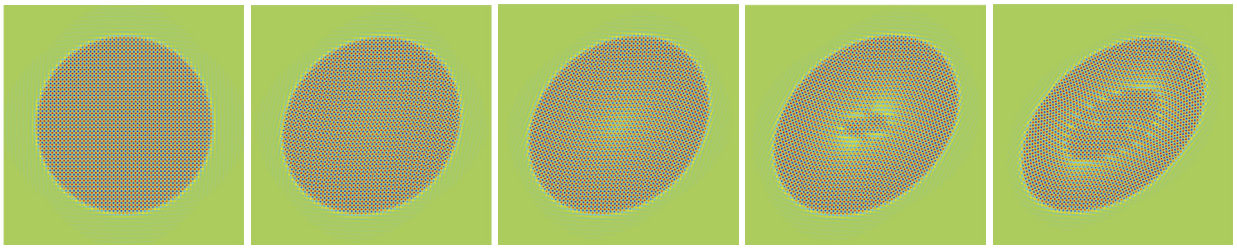

(b) Shear flow case with snapshots taken at $t = 1000$. From left to right, $u_w = 0$ (no shear) and $u_w = 3, 5, 7, 11$.

Fig. 4.4. 2D simulations of crystal growth with one initial crystal nucleus deposited at the center of the domain, in which, (a) snapshot of c at different times for the no-flow case and (b) snapshots of $\phi_1 - \phi_2$ at $t = 1000$ for various shear flow magnitude.

where $\mathscr{D}$ represents a small circular patch in the center of the domain that is given as $\mathscr{D} = \{(x, y) : \sqrt{(x-256)^2 + (y-256)^2} \leq 10\}$, $(\bar{\phi}, \zeta, q) = (0.285, 0.66, 0.446)$, and (x_l^i, y_l^i) defines a local Cartesian system obtained using local affine transformation that reads as follows:

$$(x_l^i, y_l^i) = (x\sin(\theta^i) + y\cos(\theta^i), -x\cos(\theta^i) + y\sin(\theta^i)), \tag{4.4}$$

with $\theta_i = \pm\frac{\pi}{3}$ for $i = 1, 2$. By using these two functions $\Phi_i(x, y)$ as the initial conditions, we implement EIEQ scheme for a long time ($t = 2000$) to obtain the intermediate profiles of $\hat{\Phi}_i(x, y)$.

Then, we cut out a small circular region $\mathscr{D}$ from the intermediate configuration profiles $\hat{\Phi}_i(x, y)$, and use them as the true initial conditions of $\phi_i^0(x, y)$, i.e.,

$$\phi_i^0(x, y) = \begin{cases} \hat{\Phi}_i(x, y), & \text{if } (x, y) \in \mathscr{D}, \\ \bar{\phi}, & \text{else.} \end{cases} \tag{4.5}$$

By using the initial condition $\phi_i^0, i = 1, 2$ obtained from the above process (the profile of $\phi_1^0 - \phi_2^0$ is shown in the first subfigure in Fig. 4.4), the scheme EIEQ is carried out to investigate how a small crystal nucleus evolves in the absence of the flow field. From the snapshots of $\phi_1 - \phi_2$ taken at $t = 0, 500, 1000, 1500, 1700$ shown in Fig. 4.4(a), we can see that the tiny nucleus grows gradually and forms an ordered pattern, in which two different atoms are closely aligned together to form the FCC (face-centered-cubic) lattice structure.

We further impose the shear flow on the wall boundary. For y-direction, the following shear flow boundary conditions are assumed for the velocity field $\mathbf{u} = (u, v)$:

$$u|_{(y=0,512)} = \pm u_w, v|_{(y=0,512)} = 0, \tag{4.6}$$

where u_w is the magnitude of the shear flow imposed on the wall boundary. Using the same initial conditions (4.5), we change the size of the wall velocity u_w and plot snapshots of $\phi_1 - \phi_2$ at $t = 1000$ in Fig. 4.4(b). We find that under the condition of applying a flow field, the FCC structure formed by the close arrangement of binary atoms still appears. But due to the influence of the shear flow field, the shape of the outer edge of the particles has been deformed as a whole. When the size of the shear flow field becomes larger (u_w is set as $3, 5, 7, 9$), the deformation becomes more significant.

Next, using the same method in the above example, we obtain three randomly placed crystal nuclei as the initial conditions of the seed, as shown in the first subfigure of Fig. 4.5(a). For the case which does not involve the flow field, the complete dynamic process of binary crystal growth is shown in Fig. 4.5(a). We can see that due to the different orientations of the three binary crystal nuclei, three dislocation lines have been formed and elongated over time. To show the effect of the shear flow field on crystal formation, we also plot snapshots of $\phi_1 - \phi_2$ at $t = 1000$ in Fig. 4.5(b). It can be seen that as the wall velocity u_w increases, the tilt angle of the dislocation line changes greatly, and some obvious vacancies are formed inside the cluster of binary atoms.

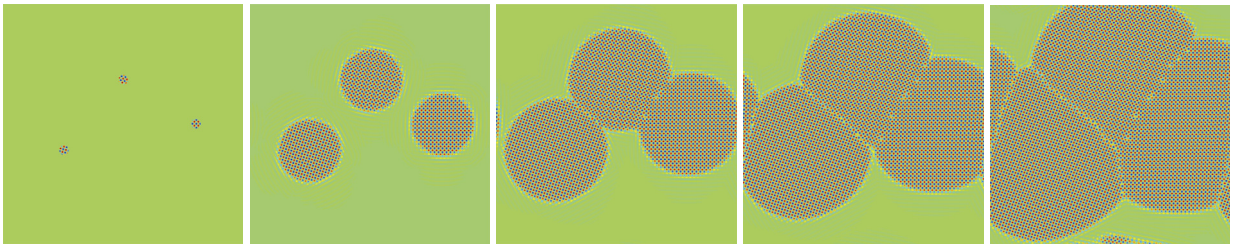

(a) No flow case, snapshots of $\phi_1 - \phi_2$ are taken at $t = 0, 400, 720, 1000, 1500$.

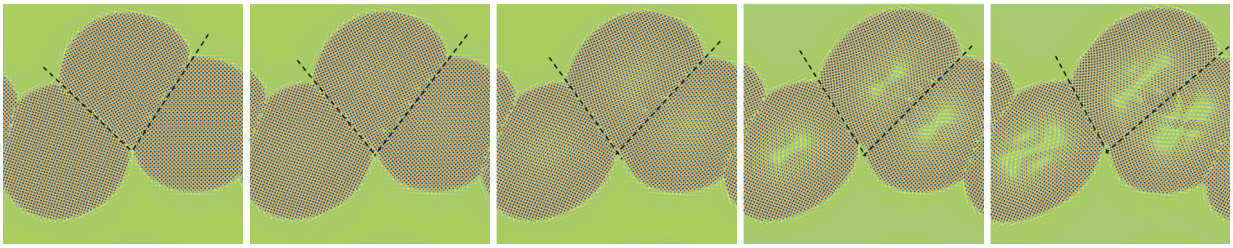

(b) Shear flow case with snapshots taken at $t = 1000$. From left to right, $u_w = 0$ (no shear) and $u_w = 3, 5, 7, 9$.

Fig. 4.5. 2D simulations of crystal growth with one initial crystal nucleus deposited at the center of the domain, in which, (a) snapshot of $\phi_1 - \phi_2$ at different times for the no-flow case and (b) snapshots of $\phi_1 - \phi_2$ at $t = 100$ for various shear flow magnitude.

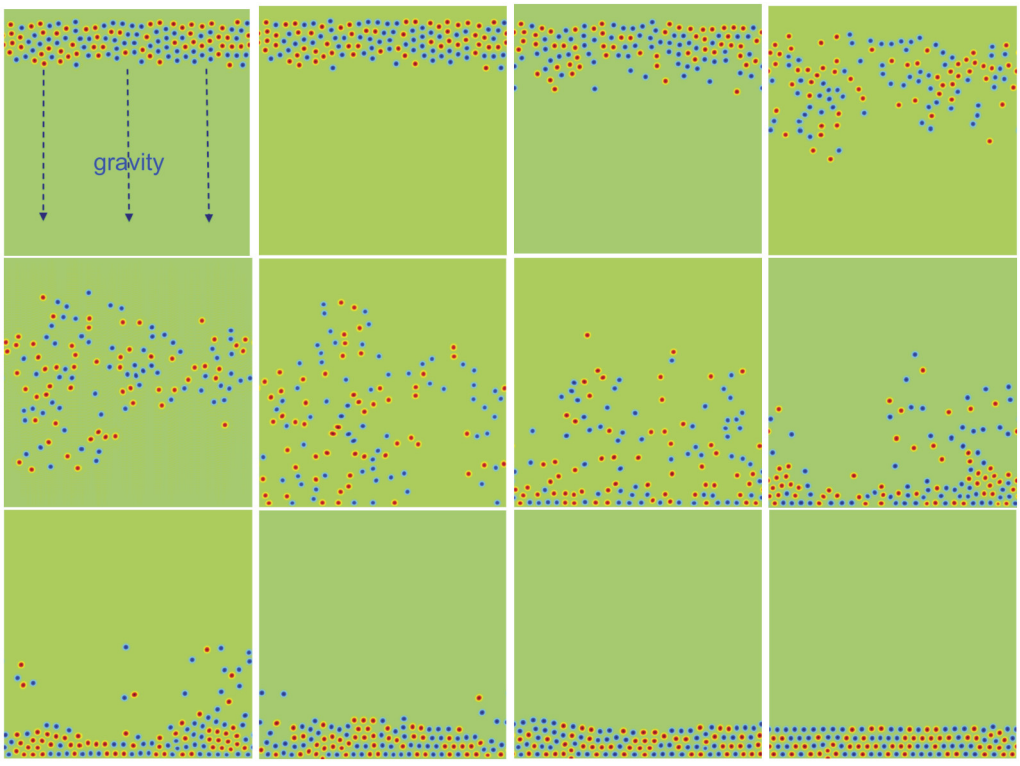

Fig. 4.6. 2D simulations of sedimentation process of many binary particles under the action of gravity force. Snapshots of $\phi_1 - \phi_2$ are plotted at $t = 0$, 200, 500, 1000, 1500, 2000, 2500, 3000, 3500, 4000, 5000, and 10000.

4.3. Sedimentation process of binary particles under gravity

In this example, using the model with the vacancy potential ($\beta \neq 0$), we numerically simulate the sedimentation process of heavier particles under the gravity force in 2D and 3D. We assume that the density difference between the crystal

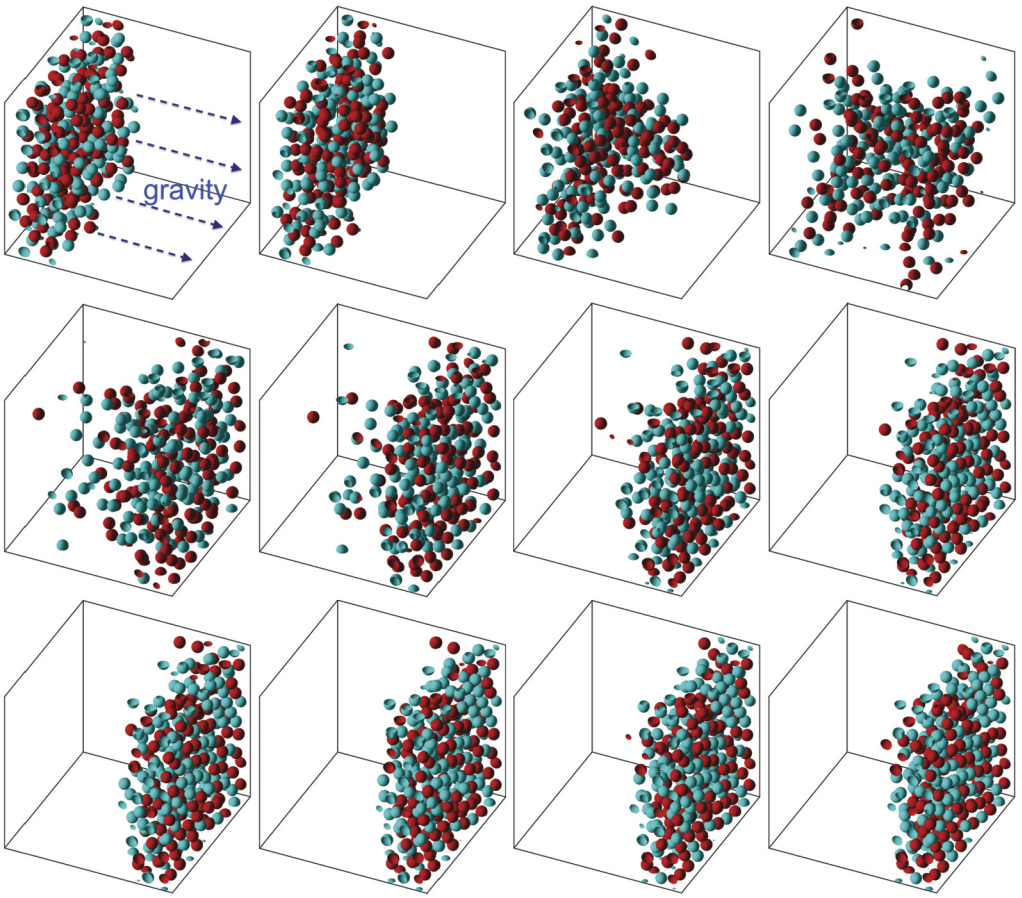

Fig. 4.7. 3D simulations of sedimentation process of many binary particles under the action of gravity force. Snapshots of the isosurfaces $\{\phi_1 = 0.3\}$ (cyan) and $\{\phi_2 = 0.3\}$ (red) are plotted at $t = 0$, 1200, 2000, 3000, 4000, 5000, 6000, 7000, 8000, 10000, 12000, and 20000.

atoms and the surrounding fluid is small, and use the so-called Boussinesq approximation to introduce gravity to the fluid momentum equation (see [45,30]). Thus, the momentum equation (2.11) is replaced by the following form

$$\mathbf{u}_t + (\mathbf{u}\cdot\nabla)\mathbf{u} - \nu\Delta\mathbf{u} + \nabla p + \phi\nabla\mu = (\rho_1 - \rho_2)\mathbf{g}_0(\phi_1 + \phi_2), \tag{4.7}$$

where $\mathbf{g}_0 = (0, g_0)$ for 2D and $\mathbf{g}_0 = (0, 0, g_0)$ for 3D, g_0 is the pre-assumed gravity constant, ρ_1 is the density of the lighter fluid medium, and ρ_2 is the density of the heavier particles.

We set the computed domain Ω to be $[0, 256]^2$ for 2D and $[0, 256]^3$ for 3D, and the model parameters to be $a_1 = a_2 = 1$, $a_{12} = 1.2$, $\varepsilon = 0.9$, $\nu = 1$, $S = 4$, $M = 1$, $\gamma = 0.5$, $\beta = 3000$, $\lambda = 0.01$, $B = 1e5$, $\delta t = 0.01$, $h = 1$. For 2D, we use the boundary conditions (2.16) along the y-direction and use the periodic boundary conditions along the x-direction. For 3D, the boundary conditions (2.16) are assumed along the z-direction and the periodic boundary conditions are used for x, y-directions.

To obtain the initial configuration of many particles near the top wall, we define the function $\Phi_i(\boldsymbol{x}), i = 1, 2$ as a constant value with small perturbations $\Phi_i(\boldsymbol{x}) = 0.07 + 0.001\text{rand}(\boldsymbol{x})$ (same as (4.2)). We implement EIEQ sufficiently long enough ($t = 2000$) to obtain the intermediate configuration profile of $\hat{\Phi}_i(\boldsymbol{x})$. Then we cut out a small strip patch D from $\hat{\Phi}_i(\boldsymbol{x})$ near the top wall, and use it as the true initial condition of $\phi_i^0(\boldsymbol{x})$, namely,

$$\phi_i^0(\boldsymbol{x}) = \begin{cases} \hat{\Phi}_i(\boldsymbol{x}), & \text{if } \boldsymbol{x} \in \mathscr{D}, \\ 0, & \text{else}, \end{cases} \tag{4.8}$$

where $\mathscr{D} = \{200 \le y \le 256\}$ for 2D and $\mathscr{D} = \{200 \le z \le 256\}$ for 3D represent the strip patch near the top.

Using the initial conditions shown in the first subfigure of Fig. 4.6 for 2D and Fig. 4.7 for 3D, we implement the developed scheme EIEQ to obtain the sedimentation dynamics of many binary particles. For 2D, snapshots of $\phi_1 - \phi_2$ are plotted at various times (shown in Fig. 4.6), where the Rayleigh-Taylor instability and fingering are observed. After long-time chaotic sedimentation, the particles finally evolve to the BCC (body-centered-cubic) structure. For 3D, we show snapshots of the isosurfaces $\{\phi_1 = 0.3\}$ and $\{\phi_2 = 0.3\}$ at various times in Fig. 4.7 as well. These obtained 2D and 3D sedimentation dynamics are consistent with the 2D simulations given in [26] using the single-phase flow-coupled PFC model, qualitatively.

5. Concluding remarks

The goals of this paper include two folds, namely, (i) we formulate the Navier-Stokes coupled binary phase-field crystal model and prove its energy law, and (ii) we design a fully discrete finite element scheme to solve the model. When designing the algorithm, we utilize special characteristics satisfied by those coupling terms (zero contribution to the dissipation law of energy). Based on this special feature, we construct special ODEs so that the original system is formulated in a form that is conducive for time discretization. In this way, the system becomes easy to be discretized, by using a linear scheme with the full decoupling structure and unconditional energy stability. We also provide a detailed practical implementation method and strictly show its solvability and energy stability. To the authors' best knowledge, the developed scheme is the first fully discrete, linear, fully decoupled algorithm for the flow-coupled phase-field crystal model, with second-order time accuracy and unconditional energy stability. Finally, we numerically demonstrate the effectiveness of the developed scheme by simulating many 2D and 3D numerical examples, including the crystal growth with/without shear flow, and sediment process of heavier binary particles.

CRediT authorship contribution statement

Xiaofeng Yang: Conceptualization, Formal analysis, Funding acquisition, Methodology, Project administration, Resources, Software, Validation, Writing – original draft. **Xiaoming He:** Conceptualization, Formal analysis, Funding acquisition, Methodology, Resources, Software, Validation, Writing – review & editing.

Declaration of competing interest

The authors declare that they have no known competing financial interests or personal relationships that could have appeared to influence the work reported in this paper.

Acknowledgements

X. Yang's work was partially supported by National Science Foundation under grant number DMS-2012490. X. He's work was partially supported by National Science Foundation under grant number DMS-1818642.

References

[1] E. Alster, K.R. Elder, J.J. Hoyt, P.W. Voorhees, Phase-field-crystal model for ordered crystals, Phys. Rev. E 95 (2017) 022105.
[2] J. Berry, M. Grant, Modeling multiple time scales during glass formation with phase-field crystals, Phys. Rev. Lett. 106 (2011) 175702.
[3] R. Backofen, A. Rätz, A. Voigt, Nucleation and growth by a phase field crystal (PFC) model, Philos. Mag. Lett. 87 (2007) 813–820.
[4] A. Baskaran, P. Zhou, Z. Hu, C. Wang, Energy stable and efficient finite-difference nonlinear multigrid schemes for the modified phase field crystal equation, J. Comput. Phys. 250 (2013) 270–292.
[5] P.Y. Chan, N. Goldenfeld, J. Dantzig, Molecular dynamics on diffusive time scales from the phase-field-crystal equation, Phys. Rev. E 79 (2009) 035701R.
[6] A.E. Diegel, X. Feng, S.M. Wise, Analysis of a mixed finite element method for a Cahn-Hilliard-Darcy-Stokes system, SIAM J. Numer. Anal. 53 (1) (2015) 127–152.
[7] W. E, J.G. Liu, Projection method. I. Convergence and numerical boundary layers, SIAM J. Numer. 32 (1995) 1017–1057.
[8] K.R. Elder, Martin Grant, Modeling elastic and plastic deformations in nonequilibrium processing using phase field crystals, Phys. Rev. E 70 (2004) 051605.
[9] K.R. Elder, Z-F. Huang, N. Provatas, Amplitude expansion of the binary phase-field-crystal model, Phys. Rev. E 81 (2010) 011602.
[10] K.R. Elder, Mark Katakowski, Mikko Haataja, Martin Grant, Modeling elasticity in crystal growth, Phys. Rev. Lett. 88 (24) (2002) 245701.
[11] K.R. Elder, N. Provatas, J. Berry, P. Stefanovic, M. Grant, Phase-field crystal modeling and classical density functional theory of freezing, Phys. Rev. B 75 (2007) 064107.
[12] K.R. Elder, K. Thornton, J.J. Hoyt, The kirkendall effect in the phase field crystal model, Philos. Mag. 91 (2011) 151–164.
[13] X. Feng, Y. He, C. Liu, Analysis of finite element approximations of a phase field model for two-phase fluids, Math. Comput. 76 (258) (2007) 539–571.
[14] Y. Gao, X.-M. He, L. Mei, X. Yang, Decoupled, linear, and energy stable finite element method for the Cahn-Hilliard-Navier-Stokes-Darcy phase field model, SIAM J. Sci. Comput. 40 (1) (2018) B110–B137.
[15] V. Girault, P.A. Raviart, Finite Element Method for Navier-Stokes Equations: Theory and Algorithms, Springer-Verlag, Berlin, Heidelberg, 1987, pp. 395–414.
[16] H. Gomez, X. Nogueira, An unconditionally energy-stable method for the phase field crystal equation, Comput. Methods Appl. Mech. Eng. 249–252 (2012) 52–61.
[17] J.L. Guermond, P. Minev, J. Shen, An overview of projection methods for incompressible flows, Comput. Methods Appl. Mech. Eng. 195 (2006) 6011–6045.
[18] Z. Hu, S.M. Wise, C. Wang, J.S. Lowengrub, Stable and efficient finite difference nonlinear-multigrid schemes for the phase field crystal equation, J. Comput. Phys. 228 (2009) 5323–5339.
[19] Q. Huang, X. Yang, X.-M. He, Numerical approximations for a smectic-a liquid crystal flow model: first-order, linear, decoupled and energy stable schemes, Discrete Contin. Dyn. Syst., Ser. B 23 (6) (2018) 2177–2192.
[20] R. Ingram, A new linearly extrapolated Crank-Nicolson time-stepping scheme for the Navier-Stokes equations, Math. Comput. 82 (284) (2013) 1953–1973.
[21] R.H. Nochetto, A.J. Salgado, I. Tomas, A diffuse interface model for two-phase ferrofluid flows, Comput. Methods Appl. Mech. Eng. 309 (2016) 497–531.
[22] R.H. Nochetto, A.J. Salgado, S.W. Walker, A diffuse interface model for electrowetting with moving contact lines, Math. Models Methods Appl. Sci. 24 (1) (2014) 67–111.
[23] Y. Peng, Y. Lu, Z. Chen, G. Yu, A binary phase field crystal study for phase segregation of liquid phase heteroepitaxial growth, Comput. Mater. Sci. 123 (2016) 65–69.

[24] I.I. Potemkin, S.V. Panyukov, Microphase separation in correlated random copolymers: mean-field theory and fluctuation corrections, Phys. Rev. E 57 (1998) 6902–6912.
[25] S. Praetorius, A. Voigt, A phase field crystal approach for particles in a flowing solvent, Macromol. Theory Simul. 20 (7) (2011) 541–547.
[26] S. Praetorius, A. Voigt, A Navier-Stokes phase-field crystal model for colloidal suspensions, J. Chem. Phys. 142 (15) (2015) 154904.
[27] Y. Qin, C. Wang, Z. Zhang, A positivity-preserving and convergent numerical scheme for the binary fluid-surfactant system, Int. J. Numer. Anal. Model. 18 (2021) 399–425.
[28] L. Rebholz, S. Wise, M. Xiao, Penalty-projection schemes for the Cahn-Hilliard Navier-Stokes diffuse interface model of two phase flow, and their connection to divergence-free coupled schemes, Int. J. Numer. Anal. Model. 15 (2018) 649–676.
[29] J. Shen, On error estimates of the projection methods for the Navier-Stokes equations: second-order schemes, Math. Comput. 65 (215) (1996) 1039–1065.
[30] J. Shen, X. Yang, Decoupled energy stable schemes for phase filed models of two phase complex fluids, SIAM J. Sci. Comput. 36 (2014) B122–B145.
[31] J. Shen, X. Yang, Decoupled, energy stable schemes for phase-field models of two-phase incompressible flows, SIAM J. Numer. Anal. 53 (1) (2015) 279–296.
[32] P. Stefanovic, M. Haataja, N. Provatas, Phase-field crystals with elastic interactions, Phys. Rev. Lett. 96 (2006) 225504.
[33] P. Stefanovic, M. Haataja, N. Provatas, Phase field crystal study of deformation and plasticity in nanocrystalline materials, Phys. Rev. E 80 (2009) 046107.
[34] J. Swift, P.C. Hohenberg, Hydrodynamic fluctuations at the convective instability, Phys. Rev. A 15 (Jan 1977) 319–328.
[35] G.I. Tóth, L. Gránásy, G. Tegze, Nonlinear hydrodynamic theory of crystallization, J. Phys. Condens. Matter 26 (2013) 055001.
[36] J. van Kan, A second-order accurate pressure-correction scheme for viscous incompressible flow, SIAM J. Sci. Stat. Comput. 7 (3) (1986) 870–891.
[37] C. Wang, S.M. Wise, An energy stable and convergent finite-difference scheme for the modified phase field crystal equation, SIAM J. Numer. Anal. 49 (2011) 945–969.
[38] S.M. Wise, C. Wang, J.S. Lowengrub, An energy-stable and convergent finite-difference scheme for the phase field crystal equation, SIAM J. Numer. Anal. 47 (3) (2009) 2269–2288.
[39] K. Wu, A. Adland, A. Karma, Phase-field-crystal model for fcc ordering, Phys. Rev. E 81 (2010) 061601.
[40] X. Yang, A new efficient fully-decoupled and second-order time-accurate scheme for Cahn-Hilliard phase-field model of three-phase incompressible flow, Comput. Methods Appl. Mech. Eng. 376 (2021) 13589.
[41] X. Yang, A novel fully-decoupled scheme with second-order time accuracy and unconditional energy stability for the Navier-Stokes equations coupled with mass-conserved Allen-Cahn phase-field model of two-phase incompressible flow, Int. J. Numer. Methods Eng. 122 (2021) 1283–1306.
[42] X. Yang, On a novel full decoupling, linear, second-order accurate, and unconditionally energy stable numerical scheme for the anisotropic phase-field dendritic crystal growth model, Int. J. Numer. Methods Eng. 122 (2021) 4129–4153.
[43] X. Yang, On a novel fully-decoupled, linear and second-order accurate numerical scheme for the Cahn-Hilliard-Darcy system of two-phase Hele-Shaw flow, Comput. Phys. Commun. 263 (2021) 107868.
[44] X. Yang, On a novel fully-decoupled, second-order accurate energy stable numerical scheme for a binary fluid-surfactant phase-field model, SIAM J. Sci. Comput. 43 (2021) B479–B507.
[45] X. Yang, J.J. Feng, C. Liu, J. Shen, Numerical simulations of jet pinching-off and drop formation using an energetic variational phase-field method, J. Comput. Phys. 218 (2006) 417–428.
[46] X. Yang, D. Han, Linearly first- and second-order, unconditionally energy stable schemes for the phase field crystal equation, J. Comput. Phys. 330 (2017) 1116–1134.
[47] X. Yang, X. He, A fully-discrete decoupled finite element method for the conserved Allen-Cahn type phase-field model of three-phase fluid flow system, Comput. Methods Appl. Mech. Eng. 389 (2022) 114376.
[48] X. Yang, J. Zhao, X.-M. He, Linear second order and unconditionally energy stable schemes for the viscous Cahn-Hilliard equation with hyperbolic relaxation using the invariant energy quadratization method, J. Comput. Appl. Math. 343 (1) (2018) 80–97.
[49] J. Zhang, X. Yang, Numerical approximations for a new L2-gradient flow based phase field crystal model with precise nonlocal mass conservation, Comput. Phys. Commun. 243 (2019) 51–67.
[50] J. Zhang, X. Yang, On efficient numerical schemes for a two-mode phase field crystal model with face-centered-cubic (FCC) ordering structure, Appl. Numer. Math. 146 (2019) 13–37.
[51] J. Zhang, X. Yang, Efficient and accurate numerical scheme for a magnetic-coupled phase-field-crystal model for ferromagnetic solid materials, Comput. Methods Appl. Mech. Eng. 371 (2020) 113110.